Atmos. Chem. Phys. Discuss., 14, 17999–18047, 2014
www.atmos-chem-phys-discuss.net/14/17999/2014/
doi:10.5194/acpd-14-17999-2014
© Author(s) 2014. CC Attribution 3.0 License.

Atmospheric Chemistry and Physics Discussions

This discussion paper is/has been under review for the journal Atmospheric Chemistry and Physics (ACP). Please refer to the corresponding final paper in ACP if available.

Multiday production of condensing organic aerosol mass in urban and forest outflow

J. Lee-Taylor[1], A. Hodzic[1], S. Madronich[1], B. Aumont[2], M. Camredon[2], and R. Valorso[2]

[1]National Center for Atmospheric Research, P.O. Box 3000, Boulder, CO 80307, USA
[2]Laboratoire Interuniversitaire des Systèmes Atmosphériques, UMR7583, CNRS, Université Paris Est Créteil et Université Paris Diderot, 94010, Créteil, France

Received: 11 May 2014 – Accepted: 6 June 2014 – Published: 3 July 2014

Correspondence to: J. Lee-Taylor (julial@ucar.edu)

Published by Copernicus Publications on behalf of the European Geosciences Union.

Abstract

Secondary organic aerosol (SOA) production in air masses containing either anthropogenic or biogenic (terpene-dominated) emissions is investigated using the explicit gas-phase chemical mechanism generator GECKO-A. Simulations show several-fold increases in SOA mass continuing for several days in the urban outflow, even as the initial air parcel is diluted into the regional atmosphere. The SOA mass increase in the forest outflow is more modest (∼ 50 %) and of shorter duration (1–2 days). The production in the urban outflow stems from continuing oxidation of gas-phase precursors which persist in equilibrium with the particle phase, and can be attributed to multigenerational reaction products of both aromatics and alkanes. In particular we find large contributions from substituted maleic anhydrides and multi-substituted peroxide-bicyclic alkenes. The results show that the predicted production is a robust feature of our model even under changing atmospheric conditions, and contradict the notion that SOA undergoes little mass production beyond a short initial formation period. The results imply that anthropogenic aerosol precursors could influence the chemical and radiative characteristics of the atmosphere over an extremely wide region, and that SOA measurements near precursor sources may routinely underestimate this influence.

1 Introduction

The contribution of anthropogenic aerosol is one of the greatest current uncertainties in the assessment of climate forcing (e.g. Forster et al., 2007). Organic aerosol (OA) comprises a significant (20–90 %) fraction of anthropogenic aerosol (Kanakidou et al., 2005; Jimenez et al., 2009; Zhang et al., 2007). OA consists, to a first approximation, of both primary organic aerosol (POA) directly emitted as particles in evaporative equilibrium with the gas phase (Robinson et al., 2007), and the much more abundant secondary organic aerosol (SOA) produced by condensation of oxidation products of gas-phase VOC (volatile organic compound) precursors (e.g. Kanakidou

ACPD
14, 17999–18047, 2014

et al., 2005; Jimenez et al., 2009). Related climate uncertainties stem from both the difficulty in characterizing the radiatively-important interactions of OA given its globally non-uniform composition (McFiggans et al., 2006), and from the difficulty in simulating its abundance and distribution (e.g Goldstein and Galbally, 2007; Hallquist et al., 2009).

Radiative impacts of atmospheric aerosols fall into two main categories, aerosol-radiation interactions and aerosol-cloud interactions (e.g. Forster et al., 2007; Boucher et al., 2013). Aerosol-radiation interactions encompass absorption and scattering of solar radiation by aerosol particles (also known as the direct effect) and cloud evaporation due to the consequent atmospheric heating (semi-direct effects). Widely different estimates of direct radiative forcing are produced by differing estimates of global SOA mass burdens (Tsigaridis, 2014; after Myhre et al., 2013; Spracklen et al., 2011). Aerosol-cloud interactions (indirect effects) encompass a range of cloud properties influenced by aerosols acting as cloud condensation nuclei (CCN). The relationship between CCN number and radiative forcing is itself complex and model parameterizations vary substantially (Boucher et al., 2013). Recent studies attribute about one-third of the total uncertainty in modeled CCN concentrations to uncertainties in SOA production (Carslaw et al., 2013), and find that CCN concentrations are sensitive to the relative proportions of POA and SOA (Trivitayanurak and Adams, 2014) and to oxidative ageing (Yu, 2011). These results show the importance of representing sources and life cycle processes that affect the mass and other climate-relevant properties of SOA in as realistic and physically-based a way as possible.

Laboratory-based descriptions of SOA formation and yields have become increasingly complex. Early calculations used precursor-specific 2-product formulations (Odum et al., 1996) which describe smog chamber OA mass yields reasonably well but produce significant underestimates of atmospheric OA in both near-source regions and in the free troposphere (e.g. Volkamer et al., 2006; Heald et al., 2011). The VBS (volatility basis set) framework (Donahue et al., 2006) uses empirical volatility (C^*) distributions to describe multi-species particle-gas mixtures and their chemical transformations (ageing) over laboratory timescales (Grieshop et al., 2009; Robinson et al., 2007). C^*

ACPD
14, 17999–18047, 2014

is the effective saturation concentration such that $C^* = C_{OA}$, the condensed concentration, when a species is equally partitioned between the gas and particle phases. This concept broadly designates SVOCs (semi-volatile organic compounds), species with significant fractions in both gas and particle phases, and IVOCs (intermediate-volatility organic compounds), gas phase species whose products are likely to condense as SOA (Donahue et al., 2009). VBS formulations have improved SOA estimates in numerous model studies e.g. (Tsimpidi et al., 2010; Lane et al., 2008; Dzepina et al., 2011; Zhang et al., 2013). However the ageing parameterizations are often tuned to match observed OA mass distributions e.g. (Jo et al., 2013), and as such are not generalizable. In efforts to incorporate more chemical complexity and realism to representations of bulk organic aerosol properties and evolution, various two-dimensional schemes have been developed e.g. (Kroll et al., 2011; Donahue et al., 2012; Pankow and Barsanti, 2009; Barsanti et al., 2013) and implemented in regional e.g. (Murphy et al., 2012) and global e.g. (Mahmud and Barsanti, 2013) models. Other model studies have increased the number of OA precursor types represented e.g. (Pye and Pouliot, 2012), or added SOA production in cloud drops e.g. (Lin et al., 2012). These modeling advances have reduced, but not eliminated the gaps between predictions and ambient measurements of SOA. While results vary, SOA in polluted regional observations tend to be underestimated even when near-urban OA observations are reproduced (Mahmud and Barsanti, 2013; Jo et al., 2013), while tropical and/or remote SOA tends to be closer to observations or even overestimated (Lin et al., 2012).

The difficulty in reproducing observed aerosol mass distributions is partly attributable to the mismatch between the timescales accessible to laboratory studies, and the atmospheric lifetimes of OA and its precursor gases. OA lifetimes are generally considered to be of the order of about a week (Boucher et al., 2013) or more (Kristiansen et al., 2012), during which the airborne particles are continually subject to ageing processes. The dynamic nature of gas-particle condensation equilibria (Pankow, 1994b) allows for evaporation–oxidation–re-condensation cycling of OA constituents, altering the chemical composition including the relative proportions of POA and SOA. In addition, the

ACPD
14, 17999–18047, 2014

continual chemical evolution of the associated gas phase implies product volatility changes on timescales of several days (Kroll and Seinfeld, 2008), opening the possibility of multi-day SOA formation. By contrast, practical considerations typically limit aerosol chamber studies to a few hours, although a few recent studies have achieved effective photochemical timescales of up to 3 days e.g. (Yee et al., 2012; Craven et al., 2012). Field observation of long-term aerosol evolution is also challenging owing to dilution and mixing of outflow plumes with regional air. SOA production in various plumes has been assessed by normalizing OA to ΔCO, the difference between plume and background CO values, e.g. DeCarlo et al. (2010) and references therein. Such observations generally extend to photochemical ages of ∼ 1 day (DeCarlo et al., 2010). Ship-borne OA and CO observations in urban plumes with transport-based ages of up to about 4 days have clearly shown SOA production for ∼ 2 days, with large data scatter thereafter (de Gouw et al., 2008).

Another problem of scale is inherent in the sheer number of potential chemical reactions and products leading to SOA formation, as compared to the bulk aerosol properties accessible from environmental chamber studies. Explicit modeling of hydrocarbon chemistry involves potentially millions of intermediate species (Aumont et al., 2005). This can be simplified to only a few hundred species when considering ozone production (Szopa et al., 2005), but is far more complicated for SOA production (Camredon et al., 2007; Valorso et al., 2011; Aumont et al., 2013, 2012) which is not dominated by any one species but rather results from condensation of many oxygenated intermediates.

The atmospheric chemical processes leading to the formation of condensable vapors and ultimately to SOA may be simulated explicitly, using structure–activity relationships based on laboratory measurements of individual and fundamental chemical kinetic rates and pathways. We have previously used the explicit model GECKO-A to simulate SOA formation in the urban outflow plume from Mexico City (Lee-Taylor et al., 2011, hereinafter LT11). That study showed OA mass production continuing for several days and yielding several times the regionally-integrated SOA mass that would be

ACPD
14, 17999–18047, 2014

implied from concentrations near the source. In this work, we use sensitivity studies and case studies with both urban and biogenic emissions assemblages to examine whether the modeled OA mass production is a robust feature of our model, and to elucidate the chemical identities of the species responsible.

2 Approach

2.1 The GECKO-A model

GECKO-A (Generator of Explicit Chemistry and Kinetics of Organics in the Atmosphere) is an automatic generator for atmospheric gas-phase chemical mechanisms. It is described in detail by Aumont et al. (2005), with updates by Camredon et al. (2007); Aumont et al. (2008); Valorso et al. (2011), and as described here. The atmospheric oxidation of aliphatic compounds is treated explicitly based directly on laboratory measurements if available, or on structure–activity relationships (SARs) where data are not available. The chemical mechanism for the oxidation of aromatic compounds is taken from the Master Chemical Mechanism, MCM v3.1 (Jenkin et al., 2003; Bloss et al., 2005a) up to the loss of the aromatic structures, and computed from GECKO-A for subsequent chemistry.

In this study we implement GECKO-A in a similar manner to that described by LT11, with the following modifications. We have implemented the SAR of Vereecken and Peeters (2009) for alkoxy decomposition rates as described in Aumont et al. (2013), we modified the SAR for hydrogen abstraction from aldehydes, based on the study by Baker et al. (2004), we added oxy radical production channels for the reactions of R-COO_2 and RO-CH_2O_2 with HO_2 (Orlando and Tyndall, 2012; Hasson et al., 2012), and we updated the branching ratios for isoprene and methacrolein oxidation (Paulot et al., 2009; Galloway et al., 2011).

Aerosol condensation in GECKO-A is based on equilibrium partitioning (Pankow, 1994a) assuming unity activity coefficients, and using published vapor pressure (P_{vap})

ACPD
14, 17999–18047, 2014

parameterizations. The model focuses on the gas-particle equilibria of products of gas-phase chemistry with a simple bulk organic aerosol phase which has no aqueous or inorganic component. We prescribe a pre-existing and non-volatile bulk seed aerosol mass to act as a condensation nucleus, as detailed below. We do not consider heterogeneous or particle-phase chemistry, nor any kinetic limitations. Here we employ the vapor pressure scheme of Nannoolal et al. (2008) together with the boiling point scheme of Nannoolal et al. (2004) (together hereinafter NAN), whereas our previous work (LT11) had used the Myrdal and Yalkowsky (1997) vapor pressure scheme which included the boiling point scheme of Joback and Reid (1987) (together hereinafter JRMY). The NAN scheme has been shown to give more realistic (and typically higher) vapor pressure results for longer-chain hydrocarbons than JRMY (Barley and McFiggans, 2010), raising the possibility (examined below) that the aerosol mass production predicted by the JRMY scheme might be an artifact. In the present study we perform a sensitivity study using both methods, to assess how the selection of vapor pressure scheme affects the predicted aerosol mass production.

2.2 Modeling scenarios

2.2.1 Urban precursors: Mexico City during MILAGRO

Our anthropogenic case study is based on the atmosphere in and near Mexico City during the MILAGRO (Megacity Initiative: Local and Global Research Observations) campaign of March 2006 (Molina et al., 2010). The emissions and initial conditions are defined similar to LT11, and briefly summarized here. Anthropogenic emissions are a mixture of light aromatics (21 % by mass), linear alkanes to C30, (44 % by mass, excluding CH_4), a selection of branched alkanes to C8 (20 % by mass) and alkenes to C6 (12 % by mass) (see Fig. 1a). Diel cycles of emission rates of chemically-similar groups with up to 10 carbons are specified following Tie et al. (2009). Emissions rates of individual species within the groups are specified according to their observed relative abundances (Apel et al., 2010). Long-chain *n*-alkanes are used as surrogates for

ACPD
14, 17999–18047, 2014

all emitted semi- and intermediate-volatility organic compounds (SVOCs and IVOCs). Their emitted masses are distributed among pre-defined volatility bins as described in LT11. The NAN scheme yields vapor pressures that are progressively higher with increasing carbon number than are those given by JRMY. Hence, the emissions distribution of individual S/IVOCs required to represent the same volatility distribution differs between the two schemes, and was therefore recalculated for NAN in this study. The carbon chain length appropriate for the 9th and lowest volatility bin in the emissions ("SVOC1", centered on $C^* = 1 \times 10^{-2}\,\mu g\,m^{-3}$) is 24–25 under the JRMY scheme but 32–33 for NAN. Precursors in this volatility bin have negligible influence on SOA mass production in LT11, since the ~ 1 % of emitted S/IVOC mass they represent partitions almost exclusively, immediately and irreversibly into the particulate phase as POA. Our current NAN simulations omit emissions from bin SVOC1 to reduce computational load, and specify emissions of *n*-alkanes up to C30, distributed among 8 volatility bins ranging from 1×10^{-1} to $1 \times 10^{6}\,\mu g\,m^{-3}$. The resulting mechanism describes 10.3 million reactions involving almost 1.8 million species and predicts vapor pressures for 0.73 million non-radicals.

2.2.2 Forest precursors: Manitou Forest during BEACHON

Our biogenic case study is based on Manitou Forest during the BEACHON-ROCS field campaign of summer 2010 (Ortega et al., 2014). The site is dominated by ponderosa pine, giving an ambient VOC mixture high in monoterpenes and low in typical anthropogenic VOCs such as aromatics, alkanes and alkenes. Emissions are represented via mixing-in of air with specified precursor concentrations based on observations (Kaser et al., 2013). The precursor mix includes selected monoterpenes (α- and β-pinene at 0.11 ppbv each, limonene at 49 pptv, and carene at 29 pptv). Specified oxygenated C1–4 species include methyl vinyl ketone at 0.25 ppbv and methyl butenol at 0.78 ppbv. Isoprene, alkanes to C6, alkenes to C5, and aromatics are also included, in the proportions shown in Fig. 1b.

ACPD
14, 17999–18047, 2014

2.3 Meteorological conditions and sensitivity studies

Our box model simulations represent photochemical evolution and aerosol condensation in an air parcel that is advected out of a source region and undergoes chemical processing during several days as part of an outflow plume. We initialize the model in the source region, in an Eulerian configuration with diurnally-varying precursor emissions, boundary layer depth, and meteorological conditions. The spin-up period in the urban scenario is driven with meteorological boundary conditions representative of average conditions in Mexico City in March 2006, as in LT11. For biogenic simulations, spin-up meteorological conditions were based on previous regional modeling studies (Cui et al., 2014). Ambient temperatures and boundary layer behavior were similar between the urban and biogenic cases. The spin-up phase lasts for just over 1.5 days, into the early afternoon of our "day 1". The model simulation then converts into a Lagrangian or outflow period, beginning at 2 p.m. in the forest case and 3 p.m. in the urban case and continuing for an additional 3 and 7 days in the forest and urban base cases respectively. Emissions cease and the air parcel (model box) maintains a fixed volume and meteorology and is subject to continuing photochemistry and to dilution with background air. Outflow period meteorological conditions are discussed below.

Throughout the model simulations we prescribe a chemically-inert background aerosol, to provide a seed for aerosol condensation. This seed aerosol is intended as a surrogate for regional background aerosol including that produced from local sources and from previous days' outflow, and contributes to the mass term in the partitioning equation (Pankow, 1994a). Seed aerosol concentration is 2 $\mu g\,m^{-3}$ in the urban case after Hodzic et al. (2009) (corresponding to 6.22×10^{9} molecules cm^{-3} at a molar weight of 200 $g\,mol^{-1}$), and 1 $\mu g\,m^{-3}$ for the forest case. Unlike species generated by GECKO-A, the inert seed stays at a constant concentration in the outflow since outflow and background concentrations are equal, hence its relative contribution to the total aerosol mass increases with dilution.

ACPD
14, 17999–18047, 2014

For each scenario we perform several sensitivity studies which are initialized with the same Eulerian conditions but diverge at the beginning of the outflow period. Our "base case" simulations continue with a constant temperature of 291 and 288 K in the urban and biogenic scenarios respectively; and a constant e-folding dilution rate k_{dil} of 1 day^{-1}. In the real world, a plume's dilution rates and air temperatures are likely to be heterogeneous, varying diurnally as well as with changing plume altitude, but such detailed variations are beyond the scope of our box model, and are represented better in three-dimensional transport models. Here we simply explore the sensitivity of our detailed photochemical and gas-particle partitioning model to these meteorological variables. Warmer temperatures should shift the equilibrium towards the gas phase, potentially reducing particle-phase mass (e.g. if aerosol-forming chemical reactions are not temperature sensitive). Our simulation denoted "T + 10 K" explores the effect on aerosol mass of an outflow temperature increased by 10 K. Plume dilution might also be expected to lead to lower particle mass, since decreasing gas-phase concentrations shift condensation equilibria in favor of evaporation. Simulation "DIL/3" is constrained similarly to the base case, however with the outflow-period dilution rate reduced to 0.3 day^{-1}. Simulation "NODIL" uses no dilution at all. Another variable governing the direction of condensation equilibrium is the existing particle mass itself, assuming that Raoult's law applies (Pankow, 1994a). Simulation "SEED/2" reduces seed aerosol mass by 50 %, starting from the beginning of the outflow period. Finally, simulation "JRMY" is meteorologically identical to the base case, but uses the JRMY vapor pressure scheme and with the S/IVOC emissions adjusted as described above. This last sensitivity study was only performed for the urban case. Details of our simulations are summarized in Table 1.

ACPD
14, 17999–18047, 2014

3 Results

3.1 Organic aerosol mass production

Figure 2 shows the development of the condensed organic aerosol generated in our set of urban and pine-forest outflow simulations. Lower panels show simulated concentrations and O/C atomic ratios. The spin-up period shows a strong diurnal cycle in response to diel variations in emissions, photolysis, and ventilation. Once the outflow period begins, particle-phase concentrations first peak in response to photochemistry then generally decline in response to dilution. On day 2 (the first full day of outflow), concentrations show an additional photochemistry-induced increase superimposed on the declining baseline, however by day 3 (the second full day of outflow) chemistry-induced concentration changes are barely discernible in either case.

To quantify the regional OA mass increase in the expanding plume, which is more relevant to net direct climate effects than is local concentration, we integrate the aerosol concentrations over the entire outflow region. Following LT11, we defined M_tOA as the organic aerosol mass in a dispersed air parcel with original volume of 1 m^3, expressed in units of µg initial m^{-3}: $M_t\mathrm{OA} = e^{tk_{\mathrm{dil}}}[\mathrm{OA}]_t$

where t is time since the start of the outflow phase. M_tOA does not include the prescribed seed aerosol which stays constant. Contrary to the progressive decreases in downwind aerosol concentrations, M_tOA increases throughout the simulation period, although the two base scenarios show very different production rate characteristics from each other. In our urban case base (Fig. 2a), M_tOA is ~6 µg initial m^{-3} at the start of the outflow phase and increases by 5–10 µg initial m^{-3} on each day of outflow. In other words, our simulated urban-outflow OA grows by a factor of 5 (to 28 µg initial m^{-3}) over 4 days. To assess the limits of this production, we continued the simulation for a further 3 days (not shown). Particle mass increased asymptotically to a maximum of 30 µg initial m^{-3}. Our forest base case (Fig. 2b) also shows particle mass production, although at a far slower rate. M_tOA begins the outflow phase at 0.8 µg m^{-3} and

ACPD
14, 17999–18047, 2014

increases by about 0.22 µg initial m^{-3} (~ 25 %) on each of the first two days of outflow. By the third day however, the production rate has slowed to only 0.03 µg initial m^{-3} (< 3 %), per day.

Figure 2 also shows particle mass development for our sensitivity simulations. The largest differences in simulated aerosol plume mass within a sensitivity case are those produced by changing the vapor pressure scheme (performed for the urban case only). Even within the city, JRMY predicts almost twice the mid-afternoon aerosol mass of NAN. Downwind, the JRMY case aerosol maintains its mass excess over the NAN case, growing by more than a factor of 3 in two days. The JRMY production slows toward the end of the simulation, whereas the NAN production continues unabated. The initial primary aerosol concentrations are very similar between the two simulations, reflecting the similar volatility distribution of the prescribed emissions. The mass production differences arise during SOA production and may be explained by the large differences in estimated P_{vap} for individual species under the two different methods. For example, estimated P_{vap} values for aromatic oxidation products are generally lower by 1–3 orders of magnitude under JRMY than under NAN. This allows JRMY to condense SOA with a lesser degree of substitution and at an earlier point in the oxidation process and explains both the early relatively rapid production in the JRMY case, and its later slowdown as the available gas phase precursors become depleted. We discuss the chemical composition of the growing aerosol in more detail later. The main result here is that the predicted OA mass production is not unique to one particular vapor pressure scheme. The following discussion refers to simulations performed with the NAN scheme only.

The response of the aerosol production rate to environmental conditions is shown in Fig. 2. In most of the sensitivity studies the organic aerosol downwind of the source region behaves much as it does in the respective base case. Particle mass in the outflow plume is rather insensitive to seed aerosol amount, dropping by no more than 6 % when the seed aerosol is reduced by 50 % (runs "SEED/2"). Raising the ambient temperature by 10 °C (runs "$T + 10$ K") lowers the condensed aerosol mass by between

ACPD
14, 17999–18047, 2014

9 and 20 % relative to the base simulation. These reductions are insufficient to lead to net mass loss in either the urban or the forest case.

Changes in dilution rate give a more complex picture. Eliminating dilution entirely (runs "NODIL") slightly increases particle mass over the base cases, whereas reducing dilution rates from 1 to 0.3 day^{-1} (runs "DIL/3") slows mass production towards the end of the urban scenario and leads to losses in the forest scenario. This non-monotonic response results from a combination of more favorable condensation at slower dilution rates (which give higher aerosol mass loadings), slower reaction rates at lower [OH], and the nonlinear response of SOA yields to [NO_x] (e.g. Camredon et al., 2007). The forest scenario has noontime [OH] representative of relatively clean air ($\sim 8 \times 10^6$ molecules cm^{-3}) in the two dilution cases, and even higher ($\sim 9 \times 10^6$ molecules cm^{-3}) in the NODIL case. [NO_x] is low in all forest cases, averaging $\sim$ 0.1–0.15 ppbv. In the urban scenario base case the high NO_x content of the urban emissions mixture leads to initial suppression of [OH], followed by daily [NO_x] reductions and [OH] increases during the outflow phase. Base case [OH] does not reach 8×10^6 molecules cm^{-3} until day 5, at daily mean NO_x levels of $\sim$ 0.4 ppbv. The OH suppression leads to delayed photochemistry in the base case urban outflow, with secondary aerosol developing later and over a more dispersed region than in the forest scenario. The urban DIL03 simulation ends with higher [NO_x] (the mean on day 5 is $\sim$ 0.5 ppbv) and lower [OH] (3×10^6 molecules cm^{-3}). The urban NODIL simulation ends with the highest diurnal mean [NO_x] (0.8 ppbv) and lowest noontime [OH] (10^6 molecules cm^{-3}). It is likely coincidental that the nonlinear response of SOA yields to the various combinations of conditions results in similar SOA mass production between the NODIL and base cases in each scenario, despite their differing chemical environments. From the point of view of our sensitivity study however, the general result is that particle phase mass integrated over the plume is only slightly sensitive to rather radical changes in the dilution rate. The mass production is therefore not an artefact of integration over a diluted plume.

ACPD
14, 17999–18047, 2014

3.2 Particle phase chemical composition and properties

The O : C atomic ratio is one of the most widely-used measures of particle chemical composition and degree of oxidation. O : C ratios for the two base case runs are shown in the lower panels of Fig. 2. O : C rises fairly steadily throughout the urban outflow simulation, from 0.16 at the start of outflow to 0.66 after 5 days and 0.72 after 7 days, indicating a particle phase that becomes progressively more oxidized with time. These values are comparable to measurements from the Mexico City area during MILAGRO (Aiken et al., 2008), although rising somewhat more slowly (see LT11). The forest case O : C ratio is higher, at 0.84 at the start of the outflow period. It then increases only slightly, ending the simulation at 0.90. This shows that the forest case particle phase is already well oxidized at the beginning of the outflow phase and undergoes little further change to its overall oxidative state. These values are somewhat higher than measurements during the BEACHON campaign, which were generally between 0.5 and 0.77, with a mean of 0.64 (Palm et al., 2013). The differences between the O : C ratio profiles in the urban and forest scenarios are consistent with delayed chemistry in the urban case outflow resulting from [OH] suppression, as described in the previous section, and with the relatively faster oxidation rates of the biogenic precursor gases.

The chemical composition of organic aerosol may also be expressed in terms of the average molecular weight per carbon (OM : OC), which includes the mass contributions of substituents such as nitrogen. Published typical OM : OC values are 1.6 ± 0.2 and 2.1 ± 0.2 for urban and nonurban areas respectively (Turpin and Lim, 2001). OM : OC for our modeled urban outflow aerosol rises from 1.41 to 2.21 over 7 days, consistent with a progression from urban to nonurban regimes, while OM : OC in our forest outflow case rises only incrementally, from 2.25 to 2.32, in agreement with the published nonurban values.

Examining the evolution of volatility of the particle phase (Fig. 3) shows that particle composition is dynamic in both the urban and forest cases. The particles progressively lose molecules of higher volatility, and gain molecules with lower volatility. The details

ACPD
14, 17999–18047, 2014

vary but the net result is that particle phase composition evolves, becoming less volatile with time. This is especially marked in the urban outflow case, where the envelope of the volatility distribution shifts to the left by two orders of magnitude. Also, the shape of the urban case volatility distribution becomes progressively more complex, due to the developing chemical composition of the particle phase (see later discussion).

Figure 4 investigates the molecular composition of the simulated particle phase, in terms of carbon number and extent of functionalization. Particles in the urban case (left hand panels) are initially composed mainly of condensed primary emissions ("POA", species with no functional groups, shown in grey) and SOA formed after one generation of chemistry (species with 1–2 functional groups, shown in red and orange) (Fig. 4a). Figure 4c shows the particle mass distribution after four days of urban outflow. Losses in the grey region centered on C26 show the evaporation of a significant fraction of the primary particle mass. This loss is balanced by a comparable gain in mono- and di-substituted species (red and orange, respectively) with the same carbon numbers, suggesting that the evaporating species re-partition to the particle phase after one generation of chemistry. A similar but smaller loss is discernible in the red region around C19, showing re-evaporation also of secondary particle mass. These model results are consistent with measurements by Miracolo et al. (2010) who also found gradual conversion of evaporating POA mass to progressively more oxidized SOA, although on a much shorter time scale in a smog chamber. At lower carbon numbers, mass production occurs after multiple generations of chemistry as shown by the production in species with ≥ 3 functional groups (yellow, green or blue). Indeed, mass gains are found at progressively lower C numbers as time progresses and more highly functionalized products become more abundant. In the forest case (right hand panels) the particle phase shows a relatively high degree of functionalization from the start of the outflow period (Fig. 4b), with most of the contributing species having ≥ 4 functional groups. Again, the particle phase adds more highly functionalized material during the outflow period (Fig. 4d) and loses small amounts of less-functionalized material. However, the

ACPD
14, 17999–18047, 2014

compositional differences between the early- and late-stage particle phases are much less marked than in the urban case.

The long-term particle phase production is much stronger in the urban outflow case than in the forest case, therefore we focus our attention on the urban case with the goal of identifying the compounds that are driving this production. We have already noted that O : C rises throughout the urban outflow simulation. Figure 5 divides the carbon mass in the growing particle phase into fractions based on O : C ratio. The figure shows that the long-term particle mass production is entirely due to more-highly substituted material, with O : C > 0.25. Furthermore, and consistent with Fig. 4, the majority of this production cannot be explained by the sequence of evaporation, oxidation and re-condensation of the less-substituted fractions, since the concurrent declines in POA and in SOA with O : C < 0.25 are comparatively small and obviously insufficient to provide the large gains seen for O : C > 0.25. The production must therefore be due to continual condensation of fresh material from the gas phase.

Figure 6 illustrates the major pathways leading to gas-particle partitioning for the urban case. The black lines represent the carbon mass in each C# bin at the start of the outflow period, with the lower line representing the phase partitioning at that time between particle (below the line) and gas (above the line). The colors of the sub-bars represent the partitioning after 4 outflow days. Brown shows particulate carbon, green shows gas phase carbon, and white shows the net carbon loss from each C# bin during the outflow period. Carbon is conserved in our model (numerical losses are of the order of 0.1 % per model day). The lost fraction in Fig. 6 represents fragmentation which reduces the C# of a molecule, moving carbon to the left and eventually off the figure into species with C# < 4. Some general trends are apparent. For the largest, least volatile molecules (C ≥ 22) virtually all the carbon partitions to the particle phase, either initially or during the outflow period. Thus, further carbon mass production in this C# range is limited to small increments from evaporation–oxidation–re-condensation cycling. The gas phase reservoir is also essentially depleted for the mid-sized molecules (with C# = 10–21). However not all the carbon has partitioned into the particle phase,

ACPD
14, 17999–18047, 2014

with a substantial portion (up to 60 %) removed by fragmentation. Some initial oxidation is usually necessary for fragmentation to occur. The competition between functionalization and fragmentation shifts in favor of increasing fragmentation for molecules with lower C# for two reasons. First, the branching ratio for CO_2 elimination from peroxy acyl radicals increases with decreasing molecular length (Chacon-Madrid et al., 2010; Arey et al., 2001), and second, longer molecules generally have lower volatility so partition earlier to the particle phase where they are protected from further gas-phase reaction (Aumont et al., 2012). For the smaller molecules (C# = 4–9) fragmentation is the major fate with only a few percent of the carbon in each bin becoming condensed. However, the much greater burden of these precursors in the outflow means that their contribution to outflow SOA is comparable to that from the mid-sized molecules, and allows substantial particle mass production despite the significant losses to fragmentation. Furthermore, a gas phase carbon reservoir persists in this size range allowing the possibility of further particle mass production, if sufficient functionalization can occur.

3.3 Chemical identity of species responsible for the production

The chemical composition of the gas-particle mixture can be explored in detail uniquely with GECKO-A, because it retains the explicit molecular identity of all intermediates and products. Figure 7 shows the time evolution of production rates for different chemical types within the urban outflow particle phase. Production rates fluctuate diurnally in response to photochemistry, showing both a daytime maximum corresponding to the solar-driven cycle in OH and a secondary production peak at sunset originating from nitrate radical chemistry. Mass losses (negative production) also have photochemically-driven diurnal cycles, with aerosol constituents re-volatilizing in response to gas phase removal. The particle phase shows production far exceeding losses for the most abundant individual secondary species and for most groups of similar species.

Figure 7 and Table 2 show that a significant proportion of the production in the urban case is attributable to only a few specific chemical species in our mechanism. Of the 20 most abundant individual species (Table 2), three in particular stand out.

ACPD
14, 17999–18047, 2014

The fastest-growing single species during daytime is hydroxy-hydroperoxy-maleic anhydride, or "MALANHYOOH". It is a major product of the oxidation of several different precursors including toluene, and its production rate is roughly correlated with the increasing trend in noontime [OH]. The chemical pathway involves unsaturated γ-dicarbonyl fragmentation products which recyclize to yield maleic anhydride and then undergo addition reactions with OH and HO_2. This species accounts for about 7 % of the particle phase by the simulation end. The fastest-growing species at nightfall is "MNNCATCOOH", a post-aromatic 4th-generation oxidation product of toluene. It is a peroxide-bicyclic alkene (hereafter denoted "PBA") with five functional groups: nitrate, nitro, hydroperoxy, and two hydroxy groups. It arises from a sequence of oxidation reactions of toluene culminating in nitrate addition to nitro-di-hydroxy toluene (nitro-catechol), which breaks the aromaticity of the molecule. Its daytime analog, "MNCATECOOH", is the nitro-hydroperoxide tri-ol, and is the second fastest-growing single species during daytime. Together these three species make up 15 % of the particle phase by the end of the simulation. They are also among the most abundant aerosol species in the forest case (Table 3) despite the relatively minor abundance of their precursors.

Many of the species in Table 2 arise directly from the aromatic mechanism, taken from the MCM rather than from subsequent chemistry generated by SARs from the GECKO-A code. Only the most favorable reaction channel is represented for each oxidation reaction in MCM, raising the possibility of over-representing the relative abundance of an individual product isomer. To address this, in Fig. 7a we summarize the behavior of products contained in this portion of the mechanism, i.e. those which retain a ring whether aromatic or otherwise. We group these species into classes with similar chemical characteristics and behaviors. Class "(M)MAL" represents the sum of MALANHYOOH and the similar methylated species MMALNHYOOH, which is the ninth-fastest contributor to particle mass production (Table 2). Class "5f-PBN" contains the five-functional PBA nitrates while class "5 + 4f-PB" represents their daytime analogs and includes a ~ 20 % contribution from the four-functional PBAs. (The mechanism contains

ACPD
14, 17999–18047, 2014

no nitrated four-functional PBAs). These two classes also include a minor contribution (< 10 %) from di-nitro PBAs formed via di-nitro cresols. Together, these three classes (M)MAL, 5f-PBN and 5 + 4f-PBN account for ∼ 30 % of the aerosol mass production during the first 4 days of the urban outflow simulation, and ∼ 40 % over 7 days. Furthermore, their relative mass contributions start small (< 5 % of aerosol mass) but become progressively greater, reaching ∼ 25 % of aerosol mass in 4 days and ∼ 30 % in 7 days. Other ring-retaining products play little role. Class "aromatics" represents all species retaining aromaticity, including substituted cresols and catechols, which are formed on day 1 but show small net losses from the particle phase over the first 4 days of outflow (∼-0.2 µg initial m^{-3}), mainly owing to losses of di-nitro-cresols. The final class in Fig. 7a is "others", encompassing epoxides, quinones, two- and three-functional PBAs, and substituted maleic anhydrides other than the two already described (see also Table 2). This group shows rapid particle-phase mass gains on day 1 in most types of its constituents, followed by largely compensating losses on subsequent days.

Particle phase production rates of all other species in the mechanism are plotted in Fig. 7b. POA shows daily net losses, while oxidized species show daily net production peaking around solar noon. We divide the oxidized species into four classes based on carbon number ("C > 7" and "C < 8") and on whether they include a nitrate or PAN moiety (designated as "N") or not ("noN"). Classes C > 7N and C > 7noN contribute 33 and 17 % respectively to net mass production, while classes C < 8N and C < 8noN contribute 16 and 5 % respectively. Production rates are strong for several days. Nitrated species show the most sustained production, slowing only on days 4 and 5 while the non-nitrated species slow to zero production 1–2 days earlier. The larger molecules (C > 7), are products of oxidation reactions of aliphatic compounds. Of these, C11–C13 species have the most rapid particle-phase production rates. The smaller molecules (C < 8) are products of sequential oxidation and fragmentation reactions of aromatic precursors, with C5 species contributing the most production. In terms of chemical identity, the species in these four classes are highly diverse, usually containing at least three different functional groups. Most C < 8 species with significant production

ACPD
14, 17999–18047, 2014

contributions contain at least one PAN or carboxylic acid group, resulting from oxidative addition to a double bond. This is not the case for the major C > 7 contributors, many of which contain δ-dicarbonyl, δ-hydroxy-hydroperoxy and/or δ-hydroxy-ketone groups resulting from 1,5 hydrogen migration in alkoxy radicals (Orlando et al., 2003). In addition to the daytime production, C < 8N species show sustained nighttime production from nitrate and peroxy chemistry.

The chemical composition of the urban case particle phase is reflected in the shape of its volatility distribution (Fig. 3a). Figure 8 distributes by half-decade in $\log_{10}(C^*)$ the major chemical classes defined above at the end of the urban simulation. Linear and branched species (classes C > 7 and C < 8) give an approximately lognormal distribution with respect to $\log_{10}(C^*)$. Superimposed on this base are peaks attributable entirely to products of aromatic chemistry. The largest peak, around $\log_{10}(C^*) = -1.5$ is due to the two substituted maleic anhydrides in class (M)MAL. The secondary peak around $\log_{10}(C^*) = -3$ results from classes 5f-PB and 5f-PBN. Class 4f-PB is more volatile, giving a small structure at $\log_{10}(C^*) \approx -0.5$, while the substituted aromatics produce only a tiny bump in the distribution, around $\log_{10}(C^*) = 2$.

The top 10 species in the forest particle phase are listed in Table 3. The biogenic precursors (α- and β-pinene, and to a lesser extent limonene, isoprene, and carene) give rise to a large variety of condensable oxidation products, as shown by the small mass contributions of even the most abundant species. The maximum individual contribution is only 2.4 %, and the top 10 species together account for < 14 % of the particle mass. The forest case aerosol is highly diverse, with species having both 4- and 6-member rings as well as ring-opened species and fragmentation products. Every species listed contains at least one hydro-peroxy group, reflecting the HO_2-dominant chemistry of this case study. Nitrated species account for about one-third of the mass. MALANHYOOH appears as the 10th most abundant aerosol species despite the comparatively low abundance of its aromatic precursors, because of its high yield. It is not present in sufficient quantity to cause long-term particle mass production, however it may be masking a decline in aerosol mass as terpene-derived products begin to decay.

ACPD
14, 17999–18047, 2014

4 Discussion and conclusions

Our results show that particle mass production in an outflow plume is a robust feature of our model. The production is largely insensitive to reasonable variations in the seed aerosol amount, temperature and dilution rate; rather it appears to be a function of the identity and photo-oxidation pathways of the chemical precursors. In our forest outflow case, high O : C ratios within the plume (Fig. 2) show that the monoterpene precursors are already well oxidized by the time the outflow portion of the simulation begins. While the gas and particle phases continue to be in dynamic equilibrium and the chemical details of their composition evolve over time, there is little change in the total particle mass in the forest case beyond the first few hours of outflow. By contrast, the initial suppression of [OH] in our urban outflow case, combined with the oxidation lifetimes of the urban precursor mix, ensures that the anthropogenic precursor mixture is only partially oxidized. The chemistry matures over several days, allowing the total particle mass to grow by a factor of > 4 outside the source region. The particle mass production results from multigenerational chemistry operating on gas phase precursors that persist in equilibrium with the particle phase even as the outflow plume dilutes into the surrounding region. In an equilibrium model, particle phase production rates necessarily reflect both gas phase production/loss rates and volatility. As species are depleted in the gas phase, our simulations also show their loss from the particle phase (e.g. in the case of the "other" aromatic compounds in Fig. 7). However, in both our urban and forest cases these losses are balanced by fresh condensation of other molecules and/or evaporation–oxidation–re-condensation, so that the particle phase volatility distribution shifts to lower vapor pressures and becomes progressively less vulnerable to re-evaporation.

The particle-phase mass production in our urban simulation is attributable in roughly equal proportion to oxidation products of light aromatic and long-chain *n*-alkane precursors. Dodecane has been shown in laboratory photo-oxidation experiments to produce SOA with fourth and higher generation products under low-NO_x conditions (Yee

ACPD
14, 17999–18047, 2014

et al., 2012; Craven et al., 2012). These experiments were performed over relatively long timescales (up to 36 h) and yielded cumulative OH exposures up to about 1×10^8 molecules cm^{-3} h, similar to the 3 day OH exposure experienced by our base case urban aerosol ($\sim 1.5 \times 10^8$ molecules cm^{-3} h). The production in aerosol mass we predict from 4- and 5-functional products of C11–C13 *n*-alkanes during the first half of our simulation is, therefore, consistent with laboratory results.

We use long-chain *n*-alkanes in this study as surrogates for the wealth of different alkane species emitted in anthropogenic situations (Isaacman et al., 2012; Fraser et al., 1997; Chan et al., 2013). This seems a reasonable approximation since *n*-alkanes have been shown in several laboratory studies (Lim and Ziemann, 2009a; Yee et al., 2013; Loza et al., 2014) to give SOA yields intermediate between those of branched and of cyclic alkanes, owing to differing OH reaction rates and to the increased (decreased) propensity of branched (cyclic) alkanes to undergo fragmentation. Our model reproduces this behavior (Aumont et al., 2013). Using a more diverse anthropogenic precursor mix from that assumed here could alter the modeled particle-phase production rates and resulting mass, in either direction, but is unlikely to eliminate the production. Therefore these qualifications do not detract from our central result that the particle phase continues to grow for several days downwind of the urban source.

We have identified two specific classes of oxidation products of light aromatics, the substituted maleic anhydrides and 5-functional peroxide-bicyclic alkenes (including those with and without nitrate), as major contributors to the SOA production especially in the later days of the simulation. Their delayed influence in the evolving urban outflow is consistent with greater SOA yields from aromatic species under low-NO_x conditions as observed by Chan et al. (2009) and Ng et al. (2007). We note that, while polycyclic aromatics are well accepted as OA precursors, light aromatics are not normally considered to be significant contributors. In the present urban outflow study, these multi-generational products together contribute roughly 30 % of the particle phase production. Admittedly, our calculations use the NAN vapor pressure scheme far beyond the list of species for which it was validated. However, even if their vapor

ACPD
14, 17999–18047, 2014

pressures are underestimated by 1–2 orders of magnitude, these products should be sufficiently involatile to partition strongly to the particle phase (see Fig. 7). We suggest that the substituted maleic anhydrides and 5-functional peroxide-bicyclic alkenes might be useful targets for observational studies seeking to validate our prediction of multiday anthropogenic aerosol production.

The fact that only a few species classes contribute such a large proportion of our predicted particle mass production also affects the volatility distribution of the developing aerosol, so that it deviates from a simple lognormal shape. If it can be shown that these species types are indeed important contributors to regional anthropogenic-origin SOA, it will be important to parameterize their volatility distributions for inclusion in regional and global models of aerosol development.

In this study we do not address loss processes that could affect the particle mass in a plume. Explicit chemistry simulations by Hodzic et al. (2013) found dry deposition to be a relatively minor factor, reducing SOA by only ∼ 15 % downwind of Mexico City. Other possible conversion processes include in-particle accretion reactions (Barsanti and Pankow, 2004), surface oxidation (Smith et al., 2009; Molina et al., 2004), photolysis (Nizkorodov et al., 2004), and multiphase chemistry (Pun and Seigneur, 2007; Ervens and Volkamer, 2010; Lim and Ziemann, 2009b), which could either increase or decrease particle mass.

If our results are generalizable to outflow from anthropogenic sources worldwide, the multiday particle mass production we predict represents a large and previously unrecognized global source, with substantial implications for the radiative forcing (RF) of climate by anthropogenic organic aerosols. For example, Smith and Bond (2014) recently attributed most RF by organic particles to human-caused biomass burning, with current annual emissions of 17.4 Tg C yr^{-1}. Their assessment relies on the assumption that these OA are purely scattering in the shortwave spectrum, with RF per unit mass comparable to that of sulfate aerosols. Our results, on the other hand, suggest a much larger regional contribution from SOA of urban origin, specifically from the use of fossil fuels comprised in large part of aromatics and long-chain alkanes. The remarkable

ACPD
14, 17999–18047, 2014

production shown in Fig. 2a would lead to a much larger anthropogenic contribution to the regional - and possibly global - burden of SOA, and their associated RF.

A crude estimate shows that large increases in anthropogenic SOA are plausible when viewed together with long-term anthropogenically-driven increases in tropospheric ozone. Northern Hemisphere (NH) tropospheric ozone has increased from pre-industrial values around 10 ppb (Volz and Kley, 1988) to 30–40 ppb (Oltmans et al., 2013). While their precise precursors and formation/removal pathways differ, both tropospheric O_3 and SOA are byproducts of the NO_x-catalyzed photo-oxidation of hydrocarbons, and are indeed highly correlated in urban observations. Examples of correlation slopes vary from 30 $\mu g\,m^{-3}\,ppm^{-1}$ in Houston to 160 $\mu g\,m^{-3}\,ppm^{-1}$ in Mexico City (e.g. Wood et al., 2010), and application of these slopes to the NH O_3 industrial-era increase would correspond to SOA concentration increases of 0.6–3.2 $\mu g\,m^{-3}$. A simple extrapolation over the entire NH in a 1 km PBL implies a hemispheric burden of 0.15–0.8 Tg, and (assuming a 10 day lifetime e.g., Kristiansen et al., 2012) an annual production rate of 5–30 Tg $year^{-1}$. Thus it is evident that regional SOA of urban origin have a large potential to modify RF on much larger scales. Unfortunately the optical properties of these SOA particles remain largely unknown; empirical evidence is mounting for strong absorption in the near UV (Kanakidou et al., 2005; Barnard et al., 2008; Lambe et al., 2013) and possibly visible wavelengths as particles age (Updyke et al., 2012), consistent with the presence of complex chromophores such as conjugated carbonyls formed by particle-phase oligomerization (which is not currently represented in our model). The combined uncertainties from the regional production and optical properties of anthropogenic SOA cast some doubt on their current representation in global models.

We note also that, in contrast to the anthropogenic SOA, biogenic SOA does not seem to show strong multiday regional production. Given that biogenics represent over 90 % of global VOC emissions, even moderate production would have had a large impact on the total SOA budget and would likely yield unrealistically high global SOA concentrations. Anthropogenic VOCs, on the other hand, are shown by our study to

ACPD
14, 17999–18047, 2014

have a potentially much larger sphere of influence than previously suspected. Of course we acknowledge many assumptions and approximations inherent in our study, and so we put forward our conclusions tentatively and semiquantitatively, but with hopefully a clear message that further study is urgently needed to resolve these issues and increase confidence in our understanding of how humans are affecting Earth's climate.

Author Contribution

J. Lee-Taylor, S. Madronich and A. Hodzic designed the study. J. Lee-Taylor and A. Hodzic performed the simulations. All co-authors contributed to model development. J. Lee-Taylor prepared the manuscript with contributions from all co-authors.

Acknowledgements. The National Center for Atmospheric Research is operated by UCAR and sponsored by the National Science Foundation. J. Lee-Taylor was supported by a grant from the US Department of Energy (Office of Science, BER, no. DE-SC0006780). B. Aumont acknowledges support from the Primequal program of the French Ministry of Ecology, Sustainable Development and Energy, the Sustainable Development Research Network (DIM-R2DS) of the Ile-de-France region and the French ANR within the project ONCEM.

References

Aiken, A. C., DeCarlo, P. F., Kroll, J. H., Worsnop, D. R., Huffman, J. A., Docherty, K. S., Ulbrich, I. M., Mohr, C., Kimmel, J. R., Sueper, D., Sun, Y., Zhang, Q., Trimborn, A., Northway, M., Ziemann, P. J., Canagaratna, M. R., Onasch, T. B., Alfarra, M. R., Prevot, A. S. H., Dommen, J., Duplissy, J., Metzger, A., Baltensperger, U., and Jimenez, J. L.: O/C and OM/OC ratios of primary, secondary, and ambient organic aerosols with high-resolution time-of-flight aerosol mass spectrometry, Environ. Sci. Technol., 42, 4478–4485, doi:10.1021/es703009q, 2008.

Apel, E. C., Emmons, L. K., Karl, T., Flocke, F., Hills, A. J., Madronich, S., Lee-Taylor, J., Fried, A., Weibring, P., Walega, J., Richter, D., Tie, X., Mauldin, L., Campos, T., Weinheimer, A., Knapp, D., Sive, B., Kleinman, L., Springston, S., Zaveri, R., Ortega, J., Voss, P.,

ACPD
14, 17999–18047, 2014

Blake, D., Baker, A., Warneke, C., Welsh-Bon, D., de Gouw, J., Zheng, J., Zhang, R., Rudolph, J., Junkermann, W., and Riemer, D. D.: Chemical evolution of volatile organic compounds in the outflow of the Mexico City Metropolitan area, Atmos. Chem. Phys., 10, 2353–2375, doi:10.5194/acp-10-2353-2010, 2010.

Arey, J., Aschmann, S. M., Kwok, E. S. C., and Atkinson, R.: Alkyl nitrate, hydroxyalkyl nitrate, and hydroxycarbonyl formation from the NO_x-air photooxidations of C-5–C-8 *n*-alkanes, J. Phys. Chem. A, 105, 1020–1027, doi:10.1021/jp003292z, 2001.

Aumont, B., Szopa, S., and Madronich, S.: Modelling the evolution of organic carbon during its gas-phase tropospheric oxidation: development of an explicit model based on a self generating approach, Atmos. Chem. Phys., 5, 2497–2517, doi:10.5194/acp-5-2497-2005, 2005.

Aumont, B., Camredon, M., Valorso, R., Lee-Taylor, J., and Madronich, S.: Development of systematic reduction techniques to describe the SOA/VOC/NO_x/O_3 system, Atmospheric Chemical Mechanisms Conference, 2008.

Aumont, B., Valorso, R., Mouchel-Vallon, C., Camredon, M., Lee-Taylor, J., and Madronich, S.: Modeling SOA formation from the oxidation of intermediate volatility *n*-alkanes, Atmos. Chem. Phys., 12, 7577–7589, doi:10.5194/acp-12-7577-2012, 2012.

Aumont, B., Camredon, M., Mouchel-Vallon, C., La, S., Ouzebidour, F., Valorso, R., Lee-Taylor, J., and Madronich, S.: Modeling the influence of alkane molecular structure on secondary organic aerosol formation, Faraday Discuss., 165, 105–122, doi:10.1039/c3fd00029j, 2013.

Baker, J., Arey, J., and Atkinson, R.: Rate constants for the gas-phase reactions of OH radicals with a series of hydroxyaldehydes at 296 ± 2 K, J. Phys. Chem. A, 108, 7032–7037, doi:10.1021/jp048979o, 2004.

Barley, M. H. and McFiggans, G.: The critical assessment of vapour pressure estimation methods for use in modelling the formation of atmospheric organic aerosol, Atmos. Chem. Phys., 10, 749–767, doi:10.5194/acp-10-749-2010, 2010.

Barnard, J. C., Volkamer, R., and Kassianov, E. I.: Estimation of the mass absorption cross section of the organic carbon component of aerosols in the Mexico City Metropolitan Area, Atmos. Chem. Phys., 8, 6665–6679, doi:10.5194/acp-8-6665-2008, 2008.

Barsanti, K. C. and Pankow, J. F.: Thermodynamics of the formation of atmospheric organic particulate matter by accretion reactions – Part 1: aldehydes and ketones, Atmos. Environ., 38, 4371–4382, doi:10.1016/j.atmosenv.2004.03.035, 2004.

ACPD
14, 17999–18047, 2014

Barsanti, K. C., Carlton, A. G., and Chung, S. H.: Analyzing experimental data and model parameters: implications for predictions of SOA using chemical transport models, Atmos. Chem. Phys., 13, 12073–12088, doi:10.5194/acp-13-12073-2013, 2013.

Bloss, C., Wagner, V., Bonzanini, A., Jenkin, M. E., Wirtz, K., Martin-Reviejo, M., and Pilling, M. J.: Evaluation of detailed aromatic mechanisms (MCMv3 and MCMv3.1) against environmental chamber data, Atmos. Chem. Phys., 5, 623–639, doi:10.5194/acp-5-623-2005, 2005a.

Bloss, C., Wagner, V., Jenkin, M. E., Volkamer, R., Bloss, W. J., Lee, J. D., Heard, D. E., Wirtz, K., Martin-Reviejo, M., Rea, G., Wenger, J. C., and Pilling, M. J.: Development of a detailed chemical mechanism (MCMv3.1) for the atmospheric oxidation of aromatic hydrocarbons, Atmos. Chem. Phys., 5, 641–664, doi:10.5194/acp-5-641-2005, 2005b.

Boucher, O., Randall, D., Artaxo, P., Bretherton, C., Feingold, G., Forster, P., Kerminen, V.-M., Kondo, Y., Liao, H., Lohmann, U., Rasch, P., Satheesh, S. K., Sherwood, S., Stevens, B., and Zhan, X. Y.: Clouds and aerosols, in: Climate Change 2013: The Physical Science Basis, Contribution of Working Group 1 to the Fifth Assessment Report of the IPCC, chap. 7, edited by: Stocker, T. F., Qin, D., Plattner, G.-K., Tignor, M., Allen, S. K., Boschung, J., Nauels, A., Xia, Y., Bex, V., and Midgley, P. M, Cambridge University Press, Cambridge, UK, and New York, NY, USA, 571–658, 2013.

Camredon, M., Aumont, B., Lee-Taylor, J., and Madronich, S.: The SOA/VOC/NO_x system: an explicit model of secondary organic aerosol formation, Atmos. Chem. Phys., 7, 5599–5610, doi:10.5194/acp-7-5599-2007, 2007.

Carslaw, K. S., Lee, L. A., Reddington, C. L., Mann, G. W., and Pringle, K. J.: The magnitude and sources of uncertainty in global aerosol, Faraday Discuss., 165, 495–512, doi:10.1039/c3fd00043e, 2013.

Chacon-Madrid, H. J., Presto, A. A., and Donahue, N. M.: Functionalization vs. fragmentation: *n*-aldehyde oxidation mechanisms and secondary organic aerosol formation, Phys. Chem. Chem. Phys., 12, 13975–13982, doi:10.1039/c0cp00200c, 2010.

Chan, A. W. H., Kautzman, K. E., Chhabra, P. S., Surratt, J. D., Chan, M. N., Crounse, J. D., Kürten, A., Wennberg, P. O., Flagan, R. C., and Seinfeld, J. H.: Secondary organic aerosol formation from photooxidation of naphthalene and alkylnaphthalenes: implications for oxidation of intermediate volatility organic compounds (IVOCs), Atmos. Chem. Phys., 9, 3049–3060, doi:10.5194/acp-9-3049-2009, 2009.

ACPD
14, 17999–18047, 2014

Chan, A. W. H., Isaacman, G., Wilson, K. R., Worton, D. R., Ruehl, C. R., Nah, T., Gentner, D. R., Dallmann, T. R., Kirchstetter, T. W., Harley, R. A., Gilman, J. B., Kuster, W. C., deGouw, J. A., Offenberg, J. H., Kleindienst, T. E., Lin, Y. H., Rubitschun, C. L., Surratt, J. D., Hayes, P. L., Jimenez, J. L., and Goldstein, A. H.: Detailed chemical characterization of unresolved complex mixtures in atmospheric organics: insights into emission sources, atmospheric processing, and secondary organic aerosol formation, J. Geophys. Res.-Atmos., 118, 6783–6796, doi:10.1002/jgrd.50533, 2013.

Craven, J. S., Yee, L. D., Ng, N. L., Canagaratna, M. R., Loza, C. L., Schilling, K. A., Yatavelli, R. L. N., Thornton, J. A., Ziemann, P. J., Flagan, R. C., and Seinfeld, J. H.: Analysis of secondary organic aerosol formation and aging using positive matrix factorization of high-resolution aerosol mass spectra: application to the dodecane low-NO_x system, Atmos. Chem. Phys., 12, 11795–11817, doi:10.5194/acp-12-11795-2012, 2012.

Cui, Y. Y., Hodzic, A., Smith, J. N., Ortega, J., Brioude, J., Matsui, H., Turnipseed, A., Winkler, P., and de Foy, B.: Modeling ultrafine particle growth at a pine forest site influenced by anthropogenic pollution during BEACHON-RoMBAS 2011, Atmos. Chem. Phys. Discuss., 14, 5611–5651, doi:10.5194/acpd-14-5611-2014, 2014.

de Gouw, J. A., Brock, C. A., Atlas, E. L., Bates, T. S., Fehsenfeld, F. C., Goldan, P. D., Holloway, J. S., Kuster, W. C., Lerner, B. M., Matthew, B. M., Middlebrook, A. M., Onasch, T. B., Peltier, R. E., Quinn, P. K., Senff, C. J., Stohl, A., Sullivan, A. P., Trainer, M., Warneke, C., Weber, R. J., and Williams, E. J.: Sources of particulate matter in the northeastern United States in summer: 1. Direct emissions and secondary formation of organic matter in urban plumes, J. Geophys. Res.-Atmos., 113, D08301, doi:10.1029/2007JD009243, 2008.

DeCarlo, P. F., Ulbrich, I. M., Crounse, J., de Foy, B., Dunlea, E. J., Aiken, A. C., Knapp, D., Weinheimer, A. J., Campos, T., Wennberg, P. O., and Jimenez, J. L.: Investigation of the sources and processing of organic aerosol over the Central Mexican Plateau from aircraft measurements during MILAGRO, Atmos. Chem. Phys., 10, 5257–5280, doi:10.5194/acp-10-5257-2010, 2010.

Donahue, N. M., Robinson, A. L., Stanier, C. O., and Pandis, S. N.: Coupled partitioning, dilution, and chemical aging of semivolatile organics, Environ. Sci. Technol., 40, 2635–2643, doi:10.1021/es052297c, 2006.

Donahue, N. M., Robinson, A. L., and Pandis, S. N.: Atmospheric organic particulate matter: from smoke to secondary organic aerosol, Atmos. Environ., 43, 94–106, doi:10.1016/j.atmosenv.2008.09.055, 2009.

ACPD
14, 17999–18047, 2014

Donahue, N. M., Kroll, J. H., Pandis, S. N., and Robinson, A. L.: A two-dimensional volatility basis set – Part 2: Diagnostics of organic-aerosol evolution, Atmos. Chem. Phys., 12, 615–634, doi:10.5194/acp-12-615-2012, 2012.

Dzepina, K., Cappa, C. D., Volkamer, R. M., Madronich, S., DeCarlo, P. F., Zaveri, R. A., and Jimenez, J. L.: Modeling the multiday evolution and aging of secondary organic aerosol during MILAGRO 2006, Environ. Sci. Technol., 45, 3496–3503, doi:10.1021/es103186f, 2011.

Ervens, B. and Volkamer, R.: Glyoxal processing by aerosol multiphase chemistry: towards a kinetic modeling framework of secondary organic aerosol formation in aqueous particles, Atmos. Chem. Phys., 10, 8219–8244, doi:10.5194/acp-10-8219-2010, 2010.

Forster, P., Ramaswamy, V., Artaxo, P., Berntsen, T., Betts, R., Fahey, D. W., Haywood, J., Lean, J., Lowe, D. C., Myhre, G., Nganga, J., Prinn, R., Raga, G., Schulz, M., and Van Dorland, R.: Changes in atmospheric constituents and in radiative forcing, in: Climate Change 2007: The Physical Science Basis, Contribution of Working Group 1 to the Fourth Assessment Report of the IPCC, chap. 2, edited by: Solomon, S., Qin, D., Manning, M., Chen, Z., Marquis, M., Averyt, K. B., Tignor, M., and Miller, H. L., Cambridge University Press, Cambridge, UK, and New York, NY, USA, 129–234, 2007.

Fraser, M. P., Cass, G. R., Simoneit, B. R. T., and Rasmussen, R. A.: Air quality model evaluation data for organics .4. C-2–C-36 non-aromatic hydrocarbons, Environ. Sci. Technol., 31, 2356–2367, 1997.

Galloway, M. M., Huisman, A. J., Yee, L. D., Chan, A. W. H., Loza, C. L., Seinfeld, J. H., and Keutsch, F. N.: Yields of oxidized volatile organic compounds during the OH radical initiated oxidation of isoprene, methyl vinyl ketone, and methacrolein under high-NO_x conditions, Atmos. Chem. Phys., 11, 10779–10790, doi:10.5194/acp-11-10779-2011, 2011.

Goldstein, A. H. and Galbally, I. E.: Known and unexplored organic constituents in the earth's atmosphere, Environ. Sci. Technol., 41, 1514–1521, 2007.

Grieshop, A. P., Logue, J. M., Donahue, N. M., and Robinson, A. L.: Laboratory investigation of photochemical oxidation of organic aerosol from wood fires 1: measurement and simulation of organic aerosol evolution, Atmos. Chem. Phys., 9, 1263–1277, doi:10.5194/acp-9-1263-2009, 2009.

Hallquist, M., Wenger, J. C., Baltensperger, U., Rudich, Y., Simpson, D., Claeys, M., Dommen, J., Donahue, N. M., George, C., Goldstein, A. H., Hamilton, J. F., Herrmann, H., Hoffmann, T., Iinuma, Y., Jang, M., Jenkin, M. E., Jimenez, J. L., Kiendler-Scharr, A., Maenhaut, W., McFiggans, G., Mentel, Th. F., Monod, A., Prévôt, A. S. H., Seinfeld, J. H., Sur-

ACPD
14, 17999–18047, 2014

ratt, J. D., Szmigielski, R., and Wildt, J.: The formation, properties and impact of secondary organic aerosol: current and emerging issues, Atmos. Chem. Phys., 9, 5155–5236, doi:10.5194/acp-9-5155-2009, 2009.

Hasson, A. S., Tyndall, G. S., Orlando, J. J., Singh, S., Hernandez, S. Q., Campbell, S., and Ibarra, Y.: Branching ratios for the reaction of selected carbonyl-containing peroxy radicals with hydroperoxy radicals, J. Phys. Chem. A, 116, 6264–6281, doi:10.1021/jp211799c, 2012.

Heald, C. L., Coe, H., Jimenez, J. L., Weber, R. J., Bahreini, R., Middlebrook, A. M., Russell, L. M., Jolleys, M., Fu, T.-M., Allan, J. D., Bower, K. N., Capes, G., Crosier, J., Morgan, W. T., Robinson, N. H., Williams, P. I., Cubison, M. J., DeCarlo, P. F., and Dunlea, E. J.: Exploring the vertical profile of atmospheric organic aerosol: comparing 17 aircraft field campaigns with a global model, Atmos. Chem. Phys., 11, 12673–12696, doi:10.5194/acp-11-12673-2011, 2011.

Hodzic, A., Jimenez, J. L., Madronich, S., Aiken, A. C., Bessagnet, B., Curci, G., Fast, J., Lamarque, J.-F., Onasch, T. B., Roux, G., Schauer, J. J., Stone, E. A., and Ulbrich, I. M.: Modeling organic aerosols during MILAGRO: importance of biogenic secondary organic aerosols, Atmos. Chem. Phys., 9, 6949–6981, doi:10.5194/acp-9-6949-2009, 2009.

Hodzic, A., Madronich, S., Aumont, B., Lee-Taylor, J., Karl, T., Camredon, M., and Mouchel-Vallon, C.: Limited influence of dry deposition of semivolatile organic vapors on secondary organic aerosol formation in the urban plume, Geophys. Res. Lett., 40, 3302–3307, doi:10.1002/grl.50611, 2013.

Isaacman, G., Chan, A. W. H., Nah, T., Worton, D. R., Ruehl, C. R., Wilson, K. R., and Goldstein, A. H.: Heterogeneous OH oxidation of motor oil particles causes selective depletion of branched and less cyclic hydrocarbons, Environ. Sci. Technol., 46, 10632–10640, doi:10.1021/es302768a, 2012.

Jenkin, M. E., Saunders, S. M., Wagner, V., and Pilling, M. J.: Protocol for the development of the Master Chemical Mechanism, MCM v3 (Part B): tropospheric degradation of aromatic volatile organic compounds, Atmos. Chem. Phys., 3, 181–193, doi:10.5194/acp-3-181-2003, 2003.

Jimenez, J. L., Canagaratna, M. R., Donahue, N. M., Prevot, A. S. H., Zhang, Q., Kroll, J. H., DeCarlo, P. F., Allan, J. D., Coe, H., Ng, N. L., Aiken, A. C., Docherty, K. S., Ulbrich, I. M., Grieshop, A. P., Robinson, A. L., Duplissy, J., Smith, J. D., Wilson, K. R., Lanz, V. A., Hueglin, C., Sun, Y. L., Tian, J., Laaksonen, A., Raatikainen, T., Rautiainen, J., Vaatto-

ACPD
14, 17999–18047, 2014

vaara, P., Ehn, M., Kulmala, M., Tomlinson, J. M., Collins, D. R., Cubison, M. J., Dunlea, E. J., Huffman, J. A., Onasch, T. B., Alfarra, M. R., Williams, P. I., Bower, K., Kondo, Y., Schneider, J., Drewnick, F., Borrmann, S., Weimer, S., Demerjian, K., Salcedo, D., Cottrell, L., Griffin, R., Takami, A., Miyoshi, T., Hatakeyama, S., Shimono, A., Sun, J. Y., Zhang, Y. M., Dzepina, K., Kimmel, J. R., Sueper, D., Jayne, J. T., Herndon, S. C., Trimborn, A. M., Williams, L. R., Wood, E. C., Middlebrook, A. M., Kolb, C. E., Baltensperger, U., and Worsnop, D. R.: Evolution of organic aerosols in the atmosphere, Science, 326, 1525–1529, doi:10.1126/science.1180353, 2009.

Jo, D. S., Park, R. J., Kim, M. J., and Spracklen, D. V.: Effects of chemical aging on global secondary organic aerosol using the volatility basis set approach, Atmos. Environ., 81, 230–244, doi:10.1016/j.atmosenv.2013.08.055, 2013.

Joback, K. G. and Reid, R. C.: Estimation of pure-component properties from group-contributions, Chem. Eng. Commun., 57, 233–243, 1987.

Kanakidou, M., Seinfeld, J. H., Pandis, S. N., Barnes, I., Dentener, F. J., Facchini, M. C., Van Dingenen, R., Ervens, B., Nenes, A., Nielsen, C. J., Swietlicki, E., Putaud, J. P., Balkanski, Y., Fuzzi, S., Horth, J., Moortgat, G. K., Winterhalter, R., Myhre, C. E. L., Tsigaridis, K., Vignati, E., Stephanou, E. G., and Wilson, J.: Organic aerosol and global climate modelling: a review, Atmos. Chem. Phys., 5, 1053–1123, doi:10.5194/acp-5-1053-2005, 2005.

Kaser, L., Karl, T., Schnitzhofer, R., Graus, M., Herdlinger-Blatt, I. S., DiGangi, J. P., Sive, B., Turnipseed, A., Hornbrook, R. S., Zheng, W., Flocke, F. M., Guenther, A., Keutsch, F. N., Apel, E., and Hansel, A.: Comparison of different real time VOC measurement techniques in a ponderosa pine forest, Atmos. Chem. Phys., 13, 2893–2906, doi:10.5194/acp-13-2893-2013, 2013.

Kristiansen, N. I., Stohl, A., and Wotawa, G.: Atmospheric removal times of the aerosol-bound radionuclides ^{137}Cs and ^{131}I measured after the Fukushima Dai-ichi nuclear accident – a constraint for air quality and climate models, Atmos. Chem. Phys., 12, 10759–10769, doi:10.5194/acp-12-10759-2012, 2012.

Kroll, J. H. and Seinfeld, J. H.: Chemistry of secondary organic aerosol: formation and evolution of low-volatility organics in the atmosphere, Atmos. Environ., 42, 3593–3624, doi:10.1016/j.atmosenv.2008.01.003, 2008.

Kroll, J. H., Donahue, N. M., Jimenez, J. L., Kessler, S. H., Canagaratna, M. R., Wilson, K. R., Altieri, K. E., Mazzoleni, L. R., Wozniak, A. S., Bluhm, H., Mysak, E. R., Smith, J. D., Kolb, C. E., and Worsnop, D. R.: Carbon oxidation state as a metric for

ACPD
14, 17999–18047, 2014

describing the chemistry of atmospheric organic aerosol, Nature Chemistry, 3, 133–139, doi:10.1038/NCHEM.948, 2011.
Lambe, A. T., Cappa, C. D., Massoli, P., Onasch, T. B., Forestieri, S. D., Martin, A. T., Cummings, M. J., Croasdale, D. R., Brune, W. H., Worsnop, D. R., and Davidovits, P.: Relationship between oxidation level and optical properties of secondary organic aerosol, Environ. Sci. Technol., 47, 6349–6357, doi:10.1021/es401043j, 2013.
Lane, T. E., Donahue, N. M., and Pandis, S. N.: Simulating secondary organic aerosol formation using the volatility basis-set approach in a chemical transport model, Atmos. Environ., 42, 7439–7451, doi:10.1016/j.atmosenv.2008.06.026, 2008.
Lee-Taylor, J., Madronich, S., Aumont, B., Baker, A., Camredon, M., Hodzic, A., Tyndall, G. S., Apel, E., and Zaveri, R. A.: Explicit modeling of organic chemistry and secondary organic aerosol partitioning for Mexico City and its outflow plume, Atmos. Chem. Phys., 11, 13219–13241, doi:10.5194/acp-11-13219-2011, 2011.
Lim, Y. B. and Ziemann, P. J.: Effects of molecular structure on aerosol yields from OH radical-initiated reactions of linear, branched, and cyclic alkanes in the presence of NO_x, Environ. Sci. Technol., 43, 2328–2334, doi:10.1021/es803389s, 2009a.
Lim, Y. B. and Ziemann, P. J.: Kinetics of the heterogeneous conversion of 1,4-hydroxycarbonyls to cyclic hemiacetals and dihydrofurans on organic aerosol particles, Phys. Chem. Chem. Phys., 11, 8029–8039, doi:10.1021/es803389s, 2009b.
Lin, G., Penner, J. E., Sillman, S., Taraborrelli, D., and Lelieveld, J.: Global modeling of SOA formation from dicarbonyls, epoxides, organic nitrates and peroxides, Atmos. Chem. Phys., 12, 4743–4774, doi:10.5194/acp-12-4743-2012, 2012.
Loza, C. L., Craven, J. S., Yee, L. D., Coggon, M. M., Schwantes, R. H., Shiraiwa, M., Zhang, X., Schilling, K. A., Ng, N. L., Canagaratna, M. R., Ziemann, P. J., Flagan, R. C., and Seinfeld, J. H.: Secondary organic aerosol yields of 12-carbon alkanes, Atmos. Chem. Phys., 14, 1423–1439, doi:10.5194/acp-14-1423-2014, 2014.
Mahmud, A. and Barsanti, K.: Improving the representation of secondary organic aerosol (SOA) in the MOZART-4 global chemical transport model, Geosci. Model Dev., 6, 961–980, doi:10.5194/gmd-6-961-2013, 2013.
McFiggans, G., Artaxo, P., Baltensperger, U., Coe, H., Facchini, M. C., Feingold, G., Fuzzi, S., Gysel, M., Laaksonen, A., Lohmann, U., Mentel, T. F., Murphy, D. M., O'Dowd, C. D., Snider, J. R., and Weingartner, E.: The effect of physical and chemical aerosol properties

ACPD
14, 17999–18047, 2014

on warm cloud droplet activation, Atmos. Chem. Phys., 6, 2593–2649, doi:10.5194/acp-6-2593-2006, 2006.
Miracolo, M. A., Presto, A. A., Lambe, A. T., Hennigan, C. J., Donahue, N. M., Kroll, J. H., Worsnop, D. R., and Robinson, A. L.: Photo-oxidation of low-volatility organics found in motor vehicle emissions: production and chemical evolution of organic aerosol mass, Environ. Sci. Technol., 44, 1638–1643, doi:10.1021/es902635c, 2010.
Molina, L. T., Madronich, S., Gaffney, J. S., Apel, E., de Foy, B., Fast, J., Ferrare, R., Herndon, S., Jimenez, J. L., Lamb, B., Osornio-Vargas, A. R., Russell, P., Schauer, J. J., Stevens, P. S., Volkamer, R., and Zavala, M.: An overview of the MILAGRO 2006 Campaign: Mexico City emissions and their transport and transformation, Atmos. Chem. Phys., 10, 8697–8760, doi:10.5194/acp-10-8697-2010, 2010.
Molina, M. J., Ivanov, A. V., Trakhtenberg, S., and Molina, L. T.: Atmospheric evolution of organic aerosol, Geophys. Res. Lett., 31, , L22104, doi:10.1029/2004gl020910, 2004.
Murphy, B. N., Donahue, N. M., Fountoukis, C., Dall'Osto, M., O'Dowd, C., Kiendler-Scharr, A., and Pandis, S. N.: Functionalization and fragmentation during ambient organic aerosol aging: application of the 2-D volatility basis set to field studies, Atmos. Chem. Phys., 12, 10797–10816, doi:10.5194/acp-12-10797-2012, 2012.
Myhre, G., Samset, B. H., Schulz, M., Balkanski, Y., Bauer, S., Berntsen, T. K., Bian, H., Bellouin, N., Chin, M., Diehl, T., Easter, R. C., Feichter, J., Ghan, S. J., Hauglustaine, D., Iversen, T., Kinne, S., Kirkevåg, A., Lamarque, J.-F., Lin, G., Liu, X., Lund, M. T., Luo, G., Ma, X., van Noije, T., Penner, J. E., Rasch, P. J., Ruiz, A., Seland, Ø., Skeie, R. B., Stier, P., Takemura, T., Tsigaridis, K., Wang, P., Wang, Z., Xu, L., Yu, H., Yu, F., Yoon, J.-H., Zhang, K., Zhang, H., and Zhou, C.: Radiative forcing of the direct aerosol effect from AeroCom Phase II simulations, Atmos. Chem. Phys., 13, 1853–1877, doi:10.5194/acp-13-1853-2013, 2013.
Myrdal, P. B. and Yalkowsky, S. H.: Estimating pure component vapor pressures of complex organic molecules, Ind. Eng. Chem. Res., 36, 2494–2499, 1997.
Nannoolal, Y., Rarey, J., Ramjugernath, D., and Cordes, W.: Estimation of pure component properties – Part 1. Estimation of the normal boiling point of non-electrolyte organic compounds via group contributions and group interactions, Fluid Phase Equilibr., 226, 45–63, 2004.
Nannoolal, Y., Rarey, J., and Ramjugernath, D.: Estimation of pure component properties – Part 3. Estimation of the vapor pressure of non-electrolyte organic compounds via group contributions and group interactions, Fluid Phase Equilibr., 269, 117–133, 2008.

ACPD
14, 17999–18047, 2014

Ng, N. L., Kroll, J. H., Chan, A. W. H., Chhabra, P. S., Flagan, R. C., and Seinfeld, J. H.: Secondary organic aerosol formation from *m*-xylene, toluene, and benzene, Atmos. Chem. Phys., 7, 3909–3922, doi:10.5194/acp-7-3909-2007, 2007.

Nizkorodov, S., Gomez, A., Lin, A., Whitt, D., and Alshawa, A.: Photodissociation action spectroscopy at organic aerosol particle–air interfaces, Abstr. Pap. Am. Chem. S., 228, U226–U226, 2004.

Odum, J. R., Hoffmann, T., Bowman, F., Collins, D., Flagan, R. C., and Seinfeld, J. H.: Gas/particle partitioning and secondary organic aerosol yields, Environ. Sci. Technol., 30, 2580–2585, 1996.

Oltmans, S. J., Lefohn, A. S., Shadwick, D., Harris, J. M., Scheel, H. E., Galbally, I., Tarasick, D. W., Johnson, B. J., Brunke, E. G., Claude, H., Zeng, G., Nichol, S., Schmidlin, F., Davies, J., Cuevas, E., Redondas, A., Naoe, H., Nakano, T., and Kawasato, T.: Recent tropospheric ozone changes – a pattern dominated by slow or no growth, Atmos. Environ., 67, 331–351, doi:10.1016/j.atmosenv.2012.10.057, 2013.

Orlando, J. J. and Tyndall, G. S.: Laboratory studies of organic peroxy radical chemistry: an overview with emphasis on recent issues of atmospheric significance, Chem. Soc. Rev., 41, 6294–6317, doi:10.1039/c2cs35166h, 2012.

Orlando, J. J., Tyndall, G. S., and Wallington, T. J.: The atmospheric chemistry of alkoxy radicals, Chem. Rev., 103, 4657–4689, doi:10.1021/cr020527p, 2003.

Ortega, J., Turnipseed, A., Guenther, A. B., Karl, T. G., Day, D. A., Gochis, D., Huffman, J. A., Prenni, A. J., Levin, E. J. T., Kreidenweis, S. M., DeMott, P. J., Tobo, Y., Patton, E. G., Hodzic, A., Cui, Y. Y., Harley, P. C., Hornbrook, R. S., Apel, E. C., Monson, R. K., Eller, A. S. D., Greenberg, J. P., Barth, M. C., Campuzano-Jost, P., Palm, B. B., Jimenez, J. L., Aiken, A. C., Dubey, M. K., Geron, C., Offenberg, J., Ryan, M. G., Fornwalt, P. J., Pryor, S. C., Keutsch, F. N., DiGangi, J. P., Chan, A. W. H., Goldstein, A. H., Wolfe, G. M., Kim, S., Kaser, L., Schnitzhofer, R., Hansel, A., Cantrell, C. A., Mauldin, R. L., and Smith, J. N.: Overview of the Manitou Experimental Forest Observatory: site description and selected science results from 2008 to 2013, Atmos. Chem. Phys., 14, 6345–6367, doi:10.5194/acp-14-6345-2014, 2014.

Palm, B. B., Ortega, A. M., Campuzano Jost, P., Day, D. A., Fry, J., Zarzana, K. J., Draper, D. C., Brown, S. S., Kaser, L., Karl, T., Jud, W., Hansel, A., Hodzic, A., Dube, W. P., Wagner, N. L., Brune, W. H., and Jimenez, J. L.: Characterizing the Amount and Chemistry of Biogenic SOA Formation from Pine Forest Air Using a Flow Reactor, poster presented at AGU Fall Meeting, San Francisco, CA, 9–13 December, A13B–0187, 2013.

ACPD
14, 17999–18047, 2014

Pankow, J. F.: An absorption-model of gas-particle partitioning of organic-compounds in the atmosphere, Atmos. Environ., 28, 185–188, doi:10.1016/1352-2310(94)90093-0, 1994a.
Pankow, J. F.: An absorption-model of the gas aerosol partitioning involved in the formation of secondary organic aerosol, Atmos. Environ., 28, 189–193, doi:10.1016/1352-2310(94)90094-9, 1994b.
Pankow, J. F. and Barsanti, K. C.: The carbon-number-polarity grid: a means to manage the-complexity of the mix of organic compounds when modeling atmospheric organic particulate matter, Atmos. Environ., 43, 2829–2835, 2009.
Paulot, F., Crounse, J. D., Kjaergaard, H. G., Kroll, J. H., Seinfeld, J. H., and Wennberg, P. O.: Isoprene photooxidation: new insights into the production of acids and organic nitrates, Atmos. Chem. Phys., 9, 1479–1501, doi:10.5194/acp-9-1479-2009, 2009.
Pun, B. K. and Seigneur, C.: Investigative modeling of new pathways for secondary organic aerosol formation, Atmos. Chem. Phys., 7, 2199–2216, doi:10.5194/acp-7-2199-2007, 2007.
Pye, H. O. T. and Pouliot, G. A.: Modeling the role of alkanes, polycyclic aromatic hydrocarbons, and their oligomers in secondary organic aerosol formation, Environ. Sci. Technol., 46, 6041–6047, doi:10.1021/es300409w, 2012.
Robinson, A. L., Donahue, N. M., Shrivastava, M. K., Weitkamp, E. A., Sage, A. M., Grieshop, A. P., Lane, T. E., Pierce, J. R., and Pandis, S. N.: Rethinking organic aerosols: semivolatile emissions and photochemical aging, Science, 315, 1259–1262, doi:10.1126/science.1133061, 2007.
Smith, J. D., Kroll, J. H., Cappa, C. D., Che, D. L., Liu, C. L., Ahmed, M., Leone, S. R., Worsnop, D. R., and Wilson, K. R.: The heterogeneous reaction of hydroxyl radicals with sub-micron squalane particles: a model system for understanding the oxidative aging of ambient aerosols, Atmos. Chem. Phys., 9, 3209–3222, doi:10.5194/acp-9-3209-2009, 2009.
Smith, S. J. and Bond, T. C.: Two hundred fifty years of aerosols and climate: the end of the age of aerosols, Atmos. Chem. Phys., 14, 537–549, doi:10.5194/acp-14-537-2014, 2014.
Spracklen, D. V., Jimenez, J. L., Carslaw, K. S., Worsnop, D. R., Evans, M. J., Mann, G. W., Zhang, Q., Canagaratna, M. R., Allan, J., Coe, H., McFiggans, G., Rap, A., and Forster, P.: Aerosol mass spectrometer constraint on the global secondary organic aerosol budget, Atmos. Chem. Phys., 11, 12109–12136, doi:10.5194/acp-11-12109-2011, 2011.
Stockwell, W. R., Kirchner, F., Kuhn, M., and Seefeld, S.: A new mechanism for regional atmospheric chemistry modeling, J. Geophys. Res.-Atmos., 22, 25847–25879, 1997.

ACPD
14, 17999–18047, 2014

Szopa, S., Aumont, B., and Madronich, S.: Assessment of the reduction methods used to develop chemical schemes: building of a new chemical scheme for VOC oxidation suited to three-dimensional multiscale HO_x–NO_x–VOC chemistry simulations, Atmos. Chem. Phys., 5, 2519–2538, doi:10.5194/acp-5-2519-2005, 2005.

Tie, X., Madronich, S., Li, G., Ying, Z., Weinheimer, A., Apel, E., and Campos, T.: Simulation of Mexico City plumes during the MIRAGE-Mex field campaign using the WRF-Chem model, Atmos. Chem. Phys., 9, 4621–4638, doi:10.5194/acp-9-4621-2009, 2009.

Trivitayanurak, W. and Adams, P. J.: Does the POA–SOA split matter for global CCN formation?, Atmos. Chem. Phys., 14, 995–1010, doi:10.5194/acp-14-995-2014, 2014.

Tsigaridis, K., Daskalakis, N., Kanakidou, M., Adams, P. J., Artaxo, P., Bahadur, R., Balkanski, Y., Bauer, S. E., Bellouin, N., Benedetti, A., Bergman, T., Berntsen, T. K., Beukes, J. P., Bian, H., Carslaw, K. S., Chin, M., Curci, G., Diehl, T., Easter, R. C., Ghan, S. J., Gong, S. L., Hodzic, A., Hoyle, C. R., Iversen, T., Jathar, S., Jimenez, J. L., Kaiser, J. W., Kirkevåg, A., Koch, D., Kokkola, H., Lee, Y. H., Lin, G., Liu, X., Luo, G., Ma, X., Mann, G. W., Mihalopoulos, N., Morcrette, J.-J., Müller, J.-F., Myhre, G., Myriokefalitakis, S., Ng, S., O'Donnell, D., Penner, J. E., Pozzoli, L., Pringle, K. J., Russell, L. M., Schulz, M., Sciare, J., Seland, Ø., Shindell, D. T., Sillman, S., Skeie, R. B., Spracklen, D., Stavrakou, T., Steenrod, S. D., Takemura, T., Tiitta, P., Tilmes, S., Tost, H., van Noije, T., van Zyl, P. G., von Salzen, K., Yu, F., Wang, Z., Wang, Z., Zaveri, R. A., Zhang, H., Zhang, K., Zhang, Q., and Zhang, X.: The AeroCom evaluation and intercomparison of organic aerosol in global models, Atmos. Chem. Phys. Discuss., 14, 6027–6161, doi:10.5194/acpd-14-6027-2014, 2014.

Tsimpidi, A. P., Karydis, V. A., Zavala, M., Lei, W., Molina, L., Ulbrich, I. M., Jimenez, J. L., and Pandis, S. N.: Evaluation of the volatility basis-set approach for the simulation of organic aerosol formation in the Mexico City metropolitan area, Atmos. Chem. Phys., 10, 525–546, doi:10.5194/acp-10-525-2010, 2010.

Turpin, B. J. and Lim, H. J.: Species contributions to $PM_{2.5}$ mass concentrations: revisiting common assumptions for estimating organic mass, Aerosol Sci. Tech., 35, 602–610, doi:10.1080/02786820152051454, 2001.

Updyke, K. M., Nguyen, T. B., and Nizkorodov, S. A.: Formation of brown carbon via reactions of ammonia with secondary organic aerosols from biogenic and anthropogenic precursors, Atmos. Environ., 63, 22–31, doi:10.1016/j.atmosenv.2012.09.012, 2012.

Valorso, R., Aumont, B., Camredon, M., Raventos-Duran, T., Mouchel-Vallon, C., Ng, N. L., Seinfeld, J. H., Lee-Taylor, J., and Madronich, S.: Explicit modelling of SOA formation from

ACPD
14, 17999–18047, 2014

α-pinene photooxidation: sensitivity to vapour pressure estimation, Atmos. Chem. Phys., 11, 6895–6910, doi:10.5194/acp-11-6895-2011, 2011.
Vereecken, L. and Peeters, J.: Decomposition of substituted alkoxy radicals-part I: a generalized structure–activity relationship for reaction barrier heights, Phys. Chem. Chem. Phys., 11, 9062–9074, doi:10.1039/b909712k, 2009.
Volkamer, R., Jimenez, J. L., San Martini, F., Dzepina, K., Zhang, Q., Salcedo, D., Molina, L. T., Worsnop, D. R., and Molina, M. J.: Secondary organic aerosol formation from anthropogenic air pollution: rapid and higher than expected, Geophys. Res. Lett., 33, L17811, doi:10.1029/2006GL026899, 2006.
Volz, A. and Kley, D.: Evaluation of the Montsouris series of ozone measurements made in the nineteenth century, Nature, 332, 240–242, doi:10.1038/332240a0, 1988.
Weininger, D.: SMILES, a chemical language and information-system .1. Introduction to methodology and encoding rules, J. Chem. Inf. Comp. Sci., 28, 31–36, doi:10.1021/ci00057a005, 1988.
Wood, E. C., Canagaratna, M. R., Herndon, S. C., Onasch, T. B., Kolb, C. E., Worsnop, D. R., Kroll, J. H., Knighton, W. B., Seila, R., Zavala, M., Molina, L. T., DeCarlo, P. F., Jimenez, J. L., Weinheimer, A. J., Knapp, D. J., Jobson, B. T., Stutz, J., Kuster, W. C., and Williams, E. J.: Investigation of the correlation between odd oxygen and secondary organic aerosol in Mexico City and Houston, Atmos. Chem. Phys., 10, 8947–8968, doi:10.5194/acp-10-8947-2010, 2010.
Yee, L. D., Craven, J. S., Loza, C. L., Schilling, K. A., Ng, N. L., Canagaratna, M. R., Ziemann, P. J., Flagan, R. C., and Seinfeld, J. H.: Secondary organic aerosol formation from low-NO_x photooxidation of dodecane: evolution of multigeneration gas-phase chemistry and aerosol composition, J. Phys. Chem. A, 116, 6211–6230, doi:10.1021/jp211531h, 2012.
Yee, L. D., Craven, J. S., Loza, C. L., Schilling, K. A., Ng, N. L., Canagaratna, M. R., Ziemann, P. J., Flagan, R. C., and Seinfeld, J. H.: Effect of chemical structure on secondary organic aerosol formation from C_{12} alkanes, Atmos. Chem. Phys., 13, 11121–11140, doi:10.5194/acp-13-11121-2013, 2013.
Yu, F.: A secondary organic aerosol formation model considering successive oxidation aging and kinetic condensation of organic compounds: global scale implications, Atmos. Chem. Phys., 11, 1083–1099, doi:10.5194/acp-11-1083-2011, 2011.
Zhang, Q., Jimenez, J. L., Canagaratna, M. R., Allan, J. D., Coe, H., Ulbrich, I., Alfarra, M. R., Takami, A., Middlebrook, A. M., Sun, Y. L., Dzepina, K., Dunlea, E., Docherty, K., De-

ACPD
14, 17999–18047, 2014

Carlo, P. F., Salcedo, D., Onasch, T., Jayne, J. T., Miyoshi, T., Shimono, A., Hatakeyama, S., Takegawa, N., Kondo, Y., Schneider, J., Drewnick, F., Borrmann, S., Weimer, S., Demerjian, K., Williams, P., Bower, K., Bahreini, R., Cottrell, L., Griffin, R. J., Rautiainen, J., Sun, J. Y., Zhang, Y. M., and Worsnop, D. R.: Ubiquity and dominance of oxygenated species in organic aerosols in anthropogenically-influenced Northern Hemisphere midlatitudes, Geophys. Res. Lett., 34, L13801, doi:10.1029/2007GL029979, 2007.

Zhang, Q. J., Beekmann, M., Drewnick, F., Freutel, F., Schneider, J., Crippa, M., Prevot, A. S. H., Baltensperger, U., Poulain, L., Wiedensohler, A., Sciare, J., Gros, V., Borbon, A., Colomb, A., Michoud, V., Doussin, J.-F., Denier van der Gon, H. A. C., Haeffelin, M., Dupont, J.-C., Siour, G., Petetin, H., Bessagnet, B., Pandis, S. N., Hodzic, A., Sanchez, O., Honoré, C., and Perrussel, O.: Formation of organic aerosol in the Paris region during the MEGAPOLI summer campaign: evaluation of the volatility-basis-set approach within the CHIMERE model, Atmos. Chem. Phys., 13, 5767–5790, doi:10.5194/acp-13-5767-2013, 2013.

ACPD
14, 17999–18047, 2014

Table 1. List of sensitivity simulations.

Name	Conditions: urban (biogenic)
Base case	T = 291 K (288 K), dilution rate = 1 day^{-1}, seed aerosol = 2 µg m^{-3} (1 µg m^{-3}), NAN vapor pressures, no dry deposition
T + 10 K	Outflow temperature = 301 K (298 K)
DIL/3	Dilution rate in outflow = 0.3 day^{-1}
SEED/2	Seed aerosol = 1 µg m^{-3} (0.5 µg m^{-3}) during outflow
JRMY	Uses JRMY vapor pressures – urban case only

ACPD
14, 17999–18047, 2014

Table 2. The top 20 contributors to modeled particle-phase production over the first 4 days[1] of the urban outflow simulation.

Rank	Formula	Unique SMILES[2] name	Class[3]	Notes/ MCM name[4]	Precursor	p_{vap} (atm)	Contribution to production Day 1	Day 4	4 days
1	$C_4H_4O_5$	OOC1C(O)C(=O)OC1=O	MMAL	MALANHYOOH	aromatics	6.1×10^{-12}	2.2 %	23.0 %	9.6 %
2	$C_7H_8O_1N_2$	CC12OOC(C1O[N](=O)=O)C(=C(O)C2(O)OO)[N](=O)=O	5f-PBN	MNNCATCOOH	toluene	1.3×10^{-13}	0.9 %	15.1 %	5.9 %
3	$C_7H_9O_9N$	CC12OOC(C1O)C(=C(O)C2(O)OO)[N](=O)=O	5f-PB	MNCATECOOH	toluene	2.6×10^{-13}	0.2 %	8.5 %	3.1 %
4	$C_5H_8O_5$	CC(=O)C(O)C(OO)C(O)=O	C < 8	fragment[5]	aromatics	2.5×10^{-11}	0.8 %	0.2 %	1.2 %
5	$C_5H_7O_9N$	OOCC(=O)C(O)C(O)C(=O)OO[N](=O)=O	C < 8,N	fragment	aromatics	2.7×10^{-12}	0.5 %	1.3 %	1.2 %
6	$C_8H_{10}O_1N_2$	CC12OOC(C)(C1O[N](=O)=O)C(O)(OO)C(=C2[N](=O)=O)O	5f-PBN	MXNNCATOOH	*m*-xylene	1.0×10^{-13}	0.4 %	1.1 %	1.1 %
7	$C_5H_8O_5$	CC(=O)C(OO)C(O)C(O)=O	C < 8	fragment	aromatics	2.5×10^{-11}	0.8 %	–	1.1 %
8	$C_8H_{10}O_1N_2$	CC1=C(O)C(O)(OO)C2(OOC1(C)C2O[N](=O)=O)[N](=O)=O	5f-PBN	OXNNCATOOH	*o*-xylene	9.5×10^{-14}	0.2 %	1.8 %	1.1 %
9	$C_5H_6O_6$	CC1(OO)OCOC(=O)C1O	MMAL	MMALNHYOOH	aromatics	5.9×10^{-12}	–	4.1 %	1.0 %
10	$C_8H_{11}O_8N$	CC1=CC(O)(OO)C2(OOC1(C)C2O)[N](=O)=O	4f-PB	TM124NOOH	1,2,4 TMB	2.9×10^{-11}	–	2.8 %	0.9 %
11	$C_7H_7O_1N_3$	CC12OOC(C=C([N](=O)=O)C1(O)OO)(C2O[N](=O)=O)[N](=O)=O	5f-PBN	NDNCRESOOH	toluene	3.0×10^{-14}	1.4 %	0.9 %	0.9 %
12	$C_5H_5O_1N_3$	OOCC(C(O[N](=O)=O)C(=O)OO[N](=O)=O)C(=O)OO[N](=O)=O	C < 8,N	fragment	aromatics	2.2×10^{-11}	1.1 %	–	0.9 %
13	$C_5H_7O_8N$	CC(=O)C(O[N](=O)=O)C(OO)C(O)=O	C < 8,N	fragment	aromatics	1.9×10^{-11}	1.5 %	0.2 %	0.8 %
14	$C_8H_{10}O_1N_2$	CC1=C(O)C(O)(OO)C2(C)OOC1(C2O[N](=O)=O)[N](=O)=O	5f-PBN	PXNNCATOOH	*p*-xylene	9.5×10^{-14}	0.2 %	1.1 %	0.7 %
15	$C_{11}H_{21}O_7N$	CCC(CCC(O)CC(=O)CCCOO)O[N](=O)=O	C > 7,N	isomers[6]	undecane	6.8×10^{-13}	0.2 %	0.9 %	0.7 %
16	$C_8H_{10}O_1N_2$	CCC12OOC(C1O[N](=O)=O)C(=C(O)C2(O)OO)[N](=O)=O	5f-PBN	ENNCATCOOH	e-benzene	3.4×10^{-14}	–	1.4 %	0.6 %
17	$C_8H_9O_1N_2$	CC1=C([N](=O)=O)C2(OOC(C)(C2O[N](=O)=O)C1(O)OO)[N](=O)=O	5f-PBN	NDNMXYLOOH	*m*-xylene	1.9×10^{-14}	–	0.5 %	0.6 %
18	$C_6H_9O_8N$	CC(=O)C(C)(OO)C(O[N](=O)=O)C(O)=O	C < 8,N	fragment	aromatics	1.3×10^{-11}	0.8 %	0.3 %	0.5 %
19	$C_7H_9O_8N$	CC12OOC(C1O)C(O)(OO)C(=C2)[N](=O)=O	4f-PB	TL4ONO2OOH	*p*-xylene	2.2×10^{-11}	–	1.6 %	0.5 %
20	$C_{12}H_{23}O_7N$	CCCC(CCC(O)CC(=O)CCCOO)O[N](=O)=O	C > 7,N	isomers	dodecane	2.0×10^{-13}	0.1 %	0.6 %	0.5 %
				Total[7] contribution to production			11.3 %	65.4 %	32.7 %

Notes:
[1] Days as used in this table are 24 h periods beginning at 4 p.m.
[2] Unique SMILES notation is based on the original definition of Weininger (1988) and referenced online at http://cactus.nci.nih.gov/translate/, February 2014.
[3] Class names are defined in the text.
[4] MCM names follow the notation of Jenkin et al. (2003); Bloss et al. (2005b), as referenced online at http://mcm.leeds.ac.uk/MCM, February 2014.
[5] Fragmentation products shown here all have several different aromatic precursors.
[6] Isomer lumping protocol is described by Valorso et al. (2011) and Aumont et al. (2008).
[7] The remainder consists of species whose individual contributions are not in the top 20.

ACPD
14, 17999–18047, 2014

Table 3. The top 10 contributors to modeled particle mass at the end of the forest outflow simulation.

Rank	Formula	Unique SMILES[1] name	Notes	Precursor	p_{vap} (atm)	Contribution to mass
1	$C_{10}H_{18}O_5$	CC1(C)C(CCO)C(OO)C1C(=O)CO	6-member ring opened	β-pinene	7.7×10^{-12}	2.4 %
2	$C_5H_{12}O_6$	CC(OO)C(O)C(CO)OO	fragment	terpenes	2.7×10^{-12}	2.0 %
3	$C_{10}H_{18}O_6$	CC(C)(C(CCO)OO)C(C=O)C(=O)CO	fully opened	β-pinene	1.8×10^{-13}	1.5 %
4	$C_{10}H_{17}O_7N$	C(C)(OO)C1CC(=O)CCC1(CO)O[N](=O)=O	4-member ring opened	β-pinene	5.8×10^{-12}	1.3 %
5	$C_5H_{12}O_6$	CC(CO)(OO)C(O)COO	fragment	limonene, isoprene	2.7×10^{-12}	1.2 %
6	$C_{10}H_{17}O_8N$	CC1(C)C2(O)CC(O[N](=O)=O)C(C)(OO)C1(C2)OO	2 rings, 4 substituents	α-, β-pinene	8.3×10^{-14}	1.2 %
7	$C_{10}H_{17}O_8N$	CC(C)(OO)C(CCC(=O)CO)CC(=O)OO[N](=O)=O	fully opened	β-pinene, limonene	5.1×10^{-12}	1.1 %
8	$C_{10}H_{17}O_7N$	CC(C)(C(CCO)O[N](=O)=O)C(C=O)C(=O)CO	fully opened	β-pinene	3.4×10^{-12}	1.1 %
9	$C_{10}H_{16}O_9N_2$	CC1(C)C2(O)CC1(CC(O[N](=O)=O)C2(C)O[N](=O)=O)OO	2 rings, 4 substituents	α-pinene	1.7×10^{-12}	1.0 %
10	$C_4H_4O_6$	OOC1C(O)C(=O)OC1=O	MALANHYOOH[2]	aromatics	6.1×10^{-12}	0.9 %
			Total contribution to mass			13.6 %

Notes: [1] Unique SMILES notation, see Table 2. [2] MCM name, as in Table 2.

ACPD
14, 17999–18047, 2014

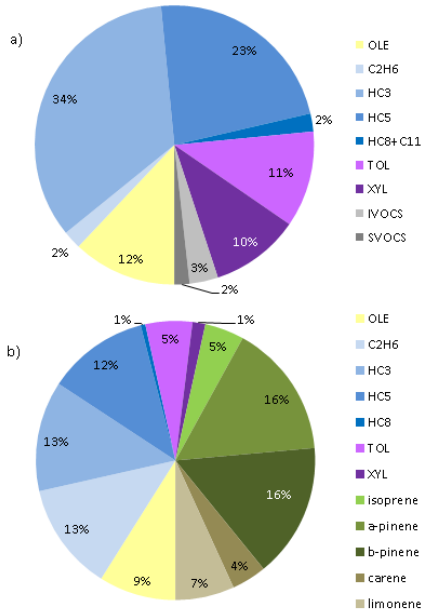

Figure 1. Precursor NMHC mass distributions for the outflow simulation runs. **(a)** Urban case emissions by mass. Total emissions are 2.6 g m^{-2} day^{-1}. Species classes correspond loosely to those of the RACM mechanism (Stockwell et al., 1997), and the volatility-based nomenclature of Donahue et al. (2009). "OLE", olefins; "C2H6", ethane; "HC3", propane and similar species ; "HC5", *n*-pentane and similar species; "HC8+C11", *n*-alkanes with 8 to 11 carbons, and cyclohexane; "TOL", toluene, benzene, and ethyl benzene; "XYL", xylenes, trimethyl benzenes, and ethyl toluene; "IVOCS", *n*-alkanes with 12 to 17 carbons; "SVOCS", *n*-alkanes with 18 to 30 carbons. Branched alkanes constitute 16 % and 66 % of the mass in classes "HC3" and "HC5" respectively. **(b)** Forest case precursor inputs. Species classes are as in **(a)**. Inputs shown total 0.23 g m^{-2} day^{-1}. Inputs of oxygenated C1–4 species are omitted for clarity, and comprise an additional 0.7 g m^{-2} day^{-1} including 0.2 g m^{-2} day^{-1} from methyl vinyl ketone and methyl butenol combined.

ACPD
14, 17999–18047, 2014

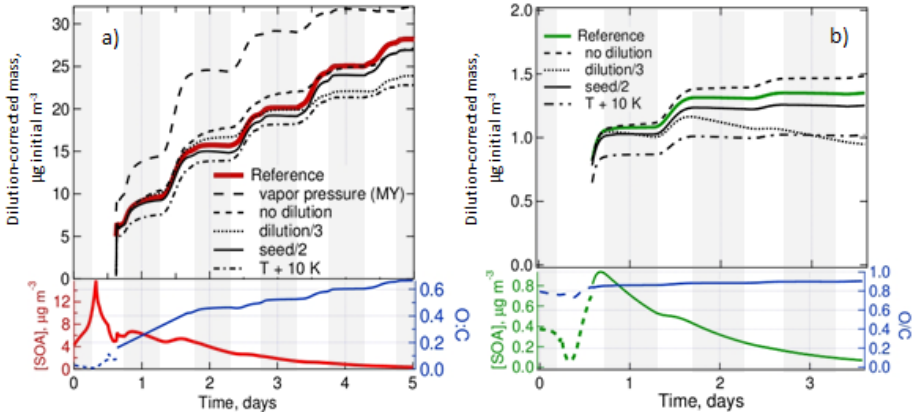

Figure 2. Simulated aerosol development for the **(a)** urban and **(b)** forest cases. Upper panels show plume-integrated mass during the outflow phase, lower panels show concentrations and O : C ratios for the source regions and outflow phases. Grey shading indicates approximate night-time periods.

ACPD
14, 17999–18047, 2014

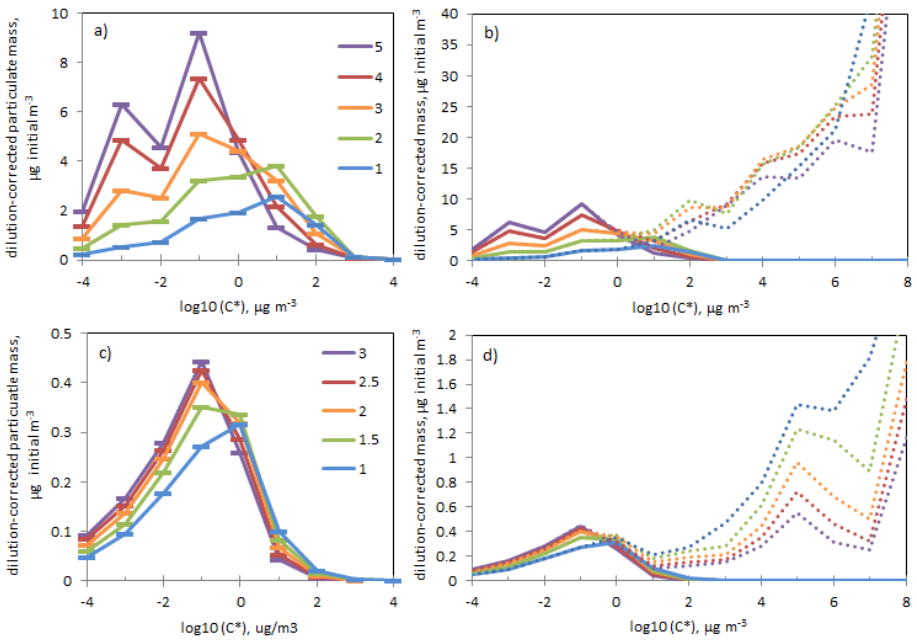

Figure 3. Time evolution of volatility distributions. **(a)** and **(b)** urban case; **(c)** and **(d)** forest case. Solid lines, particle phase; dotted lines, gas phases. Colors represent different times (see key): whole numbers are midnight values (e.g. "1" = midnight between days 1 and 2), and half-day numbers are noon values (e.g. "1.5" = noon on day 2). The volatility continuums have been binned in decadal increments for ease of comparison with so-called Volatility Basis Set (VBS) parameterizations.

ACPD
14, 17999–18047, 2014

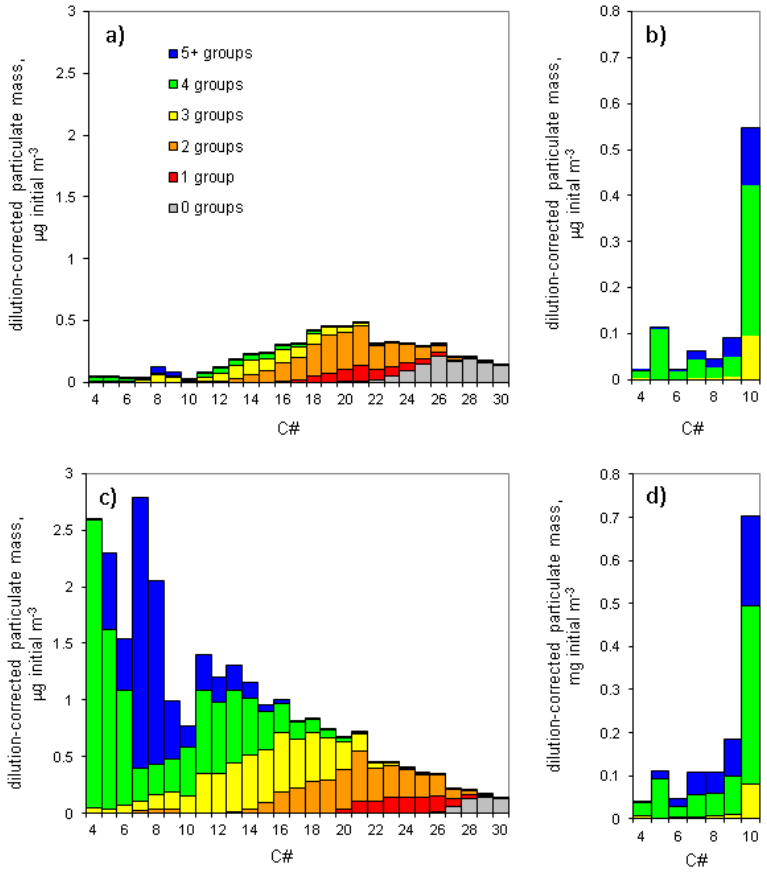

Figure 4. Particle mass composition binned by carbon number and number of functional groups per constituent molecule. **(a)** urban case at start of outflow phase; **(b)** forest case at start of outflow phase; **(c)** urban case after 4 days; **(d)** forest case after 3 days.

ACPD
14, 17999–18047, 2014

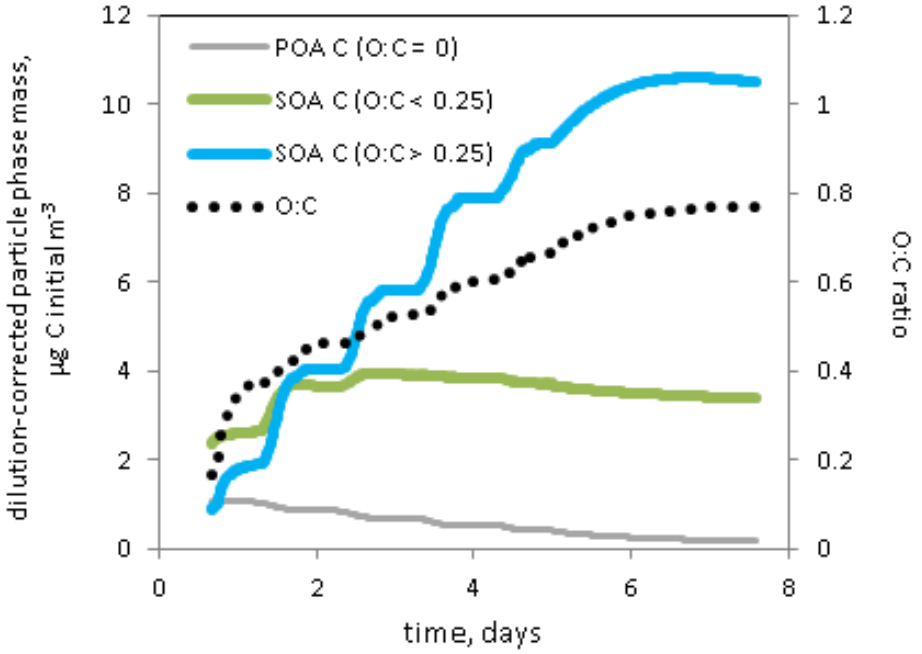

Figure 5. Evolution of the O : C ratio in the particle phase, for the urban case. Left axis and solid lines: plume-integrated carbon mass of particle phase fractions, segregated by O : C ratio. Right axis and black dotted line: O : C ratio of the entire particle phase.

ACPD
14, 17999–18047, 2014

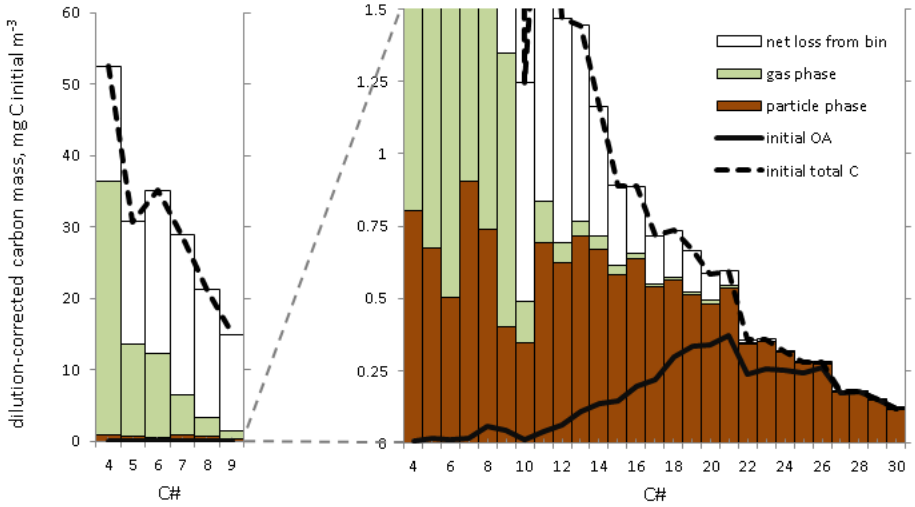

Figure 6. Carbon partitioning budget during the urban outflow simulation. Black lines show the gas (dashed line) and particle (solid line) phases at the start of outflow. Stacked bars show partitioning after 4 days: brown, particle phase; light green, persisting gas phase; white, net loss to fragmentation. Carbon numbers 4 to 9 are plotted twice, on different scales, to allow the details of the partitioning to be seen more clearly.

ACPD
14, 17999–18047, 2014

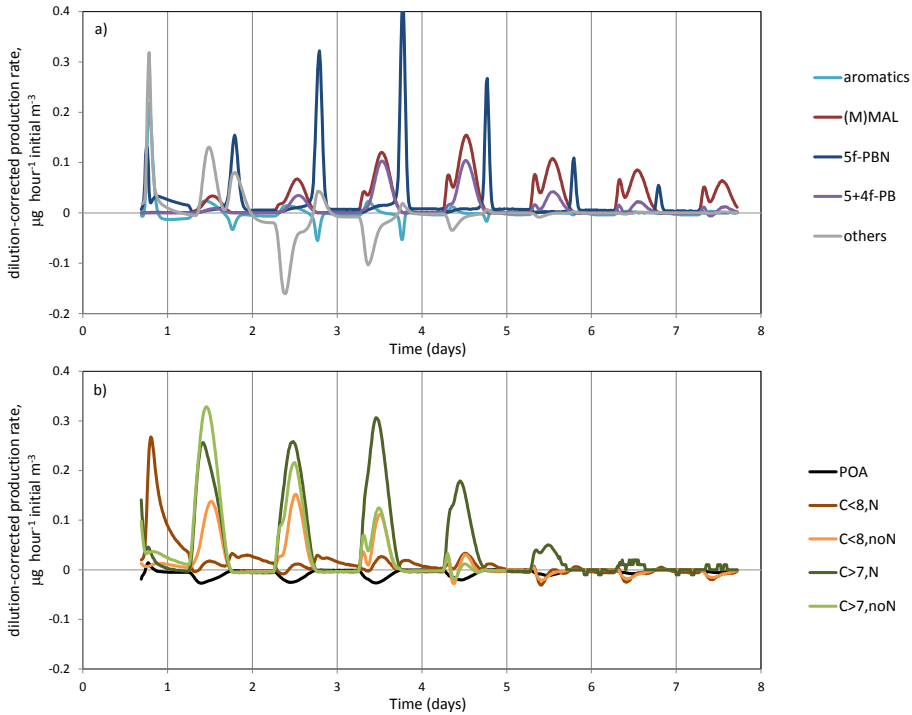

Figure 7. Hourly production rates of all species in the urban case particle phase, aggregated by broad chemical characteristics. **(a)** Cyclic products of aromatic precursors; **(b)** all other species. Colors show species groupings. See text for details.

ACPD
14, 17999–18047, 2014

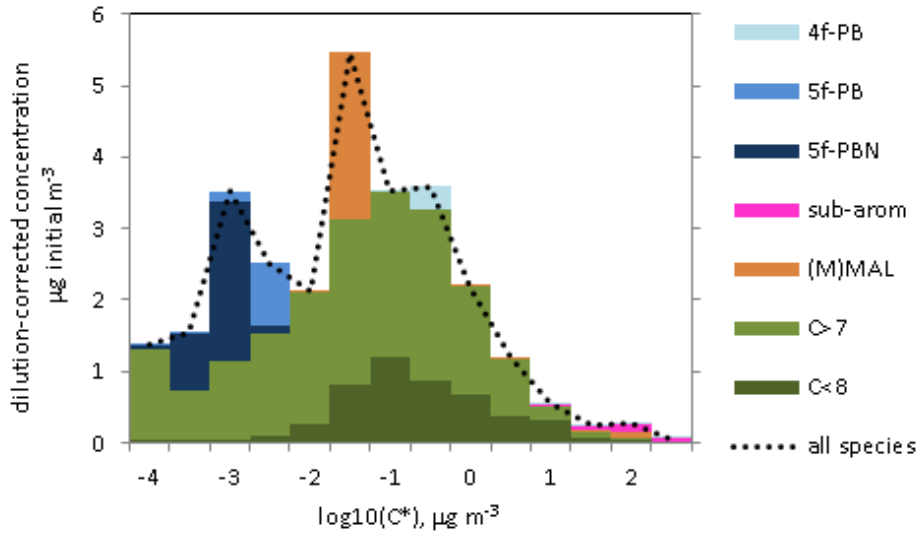

Figure 8. Chemical composition of the particle phase at the end of day 5 of the urban outflow simulation, distributed by volatility. Colors show species groupings as discussed in the text: "C < 8" and "C > 7", linear/branched molecules separated by carbon number (no distinction for nitrate is made here); "(M)MAL", substituted maleic anhydrides; "sub-arom", substituted rings that retain aromaticity; "5f-PBN", PBAs with 5 functional groups including nitrate; "5f-PB", as 5f-PBN without nitrate; "4f-PB", PBAs with 4 functional groups. Dotted line shows total particle phase mass. The leftmost bin also includes the mass from species with $\log_{10}(C^*) < -4$.

ACPD
14, 17999–18047, 2014